Journal of Advances in Mathematics and Computer Science

Volume 39, Issue 2, Page 20-51, 2024; Article no.JAMCS.110718

ISSN: 2456-9968

(Past name: British Journal of Mathematics & Computer Science, Past ISSN: 2231-0851)

Global Stability Analysis of a Fractional-Order Ebola Epidemic Model with Control Strategies

Paride O. Lolika [a*], Mlyashimbi Helikumi [b], Sulieman A. S. Jomah [a], Mohamed Y. A. Bakhet [c], Kennedy Crispo Galla [d] and Awad Hussien Kheiralla [d]

[a] *University of Juba, Department of Mathematics, P.O. Box 82 Juba, Central Equatoria, South Sudan.*

[b] *Mbeya University of Science and Technology, Department of Mathematics and Statistics, College of Science and Technical Education, P.O. Box 131, Mbeya, Tanzania.*

[c] *University of Juba, School of Mathematics, P.O. Box 82 Juba, Central Equatoria, South Sudan.*

[d] *University of Juba, Department of Biology, P.O. Box 82 Juba, Central Equatoria, South Sudan.*

Authors' contributions

This work was carried out in collaboration among all authors. All authors read and approved the final manuscript.

Article Information

DOI: 10.9734/JAMCS/2024/v39i21866

Open Peer Review History:

This journal follows the Advanced Open Peer Review policy. Identity of the Reviewers, Editor(s) and additional Reviewers, peer review comments, different versions of the manuscript, comments of the editors, etc are available here: http://www.sdiarticle5.com/review-history/110718

Original Research Article

Received: 17/11/2023

Accepted: 22/01/2024

Published: 13/02/2024

Abstract

We proposed a fractional-order derivative model for Ebola virus disease (EVD) to assess the effects of control strategies on the spread of the disease in the population. The proposed model incorporates all relevant biological factors, health education campaigns, prevention measures, and treatment as control strategies. We computed the basic reproduction number $\mathcal{R}_0$ and qualitatively used it to assess the existence of the model states. In particular, we noted that two equilibrium points exist, the disease-free and endemic equilibrium points which are both globally stable whenever $\mathcal{R}_0 < 1$ and $\mathcal{R}_0 > 1$ respectively. We performed sensitivity

**Corresponding author: E-mail: parideoresto@yahoo.com;*

analysis on the key parameters that drive the EVD dynamics to determine their relative importance in EVD transmission and prevalence. Model parameters were estimated using the 2014 Ebola outbreak in Guinea. Further, numerical simulation results are presented using fractional Adam-Bashforth-Moulton scheme to support the analytical findings. From the numerical simulations, we have noted that as α decreases from unit, the solution profiles of the model attain its stability much faster than at $\alpha = 1$. Furthermore, the results demonstrated that the aforementioned control strategies have the potential to reduce the transmission of EVD in the population.

Keywords: Lyapunov; control strategies; Ebola model; fractional-order derivatives; model stability; data fitting; model validation.

2010 Mathematics Subject Classification: 53C25, 83C05, 57N16.

1 Introduction

Ebola virus disease (EVD) is a disease caused by Ebola virus in humans and other non-human primates like gorillas, chimpanzees and duikers. The virus originated in fruit bats and jumped to humans through animals such as chimpanzees [1, 2]. The disease first appeared in 1976 in two outbreaks, one in Sudan and the other in Democratic Republic of Congo (DRC). Since then, the disease has continued to appear in Africa several times, for example, in Ivory Coast and Gabon in 1994; in Uganda in 2000; in Guinea in 2014; and again in DRC in 2019.

The EVD outbreaks, particularly in Western part of Africa, continue to present substantial challenges to health and health-care resources in the region and beyond. According to the World Health organization (WHO), more than 11000 people died in the region between 2013 and 2016 due to the outbreak of EVD [3]. In particular, Sierra Leone alone recorded more than 14,100 Ebola cases which resulted in over 3900 deaths, and more than 30000 individuals were quarantined due to possible Ebola exposure [4].

Although several factors such as poor health facilities and highly populated urban areas have been attributed to perpetuate EVD during an outbreak, funeral and burial practices anchored in certain traditional and religious practices of the West African communities are regarded as one of the leading factors that fuel the spread of EVD in the region [5, 6]. As most communities in West Africa believe in life after death, funeral and burial practices are given a lot of significance and perceived as crucial steps in transitioning from the world of the living to the spiritual world [7]. Individuals from this region believe that the transition should be facilitated by surviving relatives through funeral and burial rituals. Communities perceive that if the deceased does not attain the elevated rank of ancestral spirit, their spirit may return and punish the living relatives [6]. Hence, several unique funeral and burial practices that more often involve excessive contact with a corpse are often performed to appease the dead. In its global alert and response report of WHO concurred with this assertion by suggesting that nearly 60% of all Ebola cases in Guinea between 2013 and 2014 were a result of traditional burial practices [8]. Cognizant of this, it is essential to gain a better and more comprehensive understanding of the impact of funeral and burial practices during EVD outbreaks to develop feasible intervention and management strategies. Among the several tools and techniques that can be used to explore this phenomenon is mathematical modeling.

Mathematical modelling, as a powerful tool in quantifying the complex and numerous factors, has been widely developed to explore the transmission of EVD [9, 10, 11]. Mathematical modeling is described as the conversion of a real problem in a mathematical form. Modeling, therefore, involves the formulation of the real-life situations or converting the problems in mathematical explanations to a real or believable situation (see for example [12, 13].

Mathematical models with classical-order differential equations have especially received great attention (see, [14, 15, 16, 17, 18, 19, 20, 21, 22]) and have widely been used in disease modeling. However, recent studies suggest that models with integer-order derivatives do not adequately capture hereditary properties, long-range interactions, and memory effects that exist in biological systems which have many applications in the fields of

science, compared to fractional-order derivatives [23, 24, 25, 26, 27]. It is documented literature that models that utilize fractional-order derivatives capture hereditary properties, memory effects, and enlarge the region of stability [27]. Previous studies suggest that without memory effects evolution and control of diseases in communities can not be considered [28]. In particular, whenever the disease spreads in societies, humans gain experience which influence in control of spread disease in the community [27, 29]. Additionally, cell membrane of living organisms contain some fractional order-electrical conductance which are classified in groups of fractional order models [23, 28].

Recently, Ivan et al. [30], Muhammad et al. [31], Dokuyucua and Dutta [32], Farman et al.[33], Singh[34] and Pan et al. [35] used the fractional-order derivatives to study the effect of memory on EVD dynamics. Dokuyucua and Dutta [32] utilised Caputo fractional-order differential equations without singular kernel to explore the effects of memory on spread of Ebola in Africa. Among several other outcomes, they found out that their model solutions were in agreement with reality. Muhammad et al. [31] proposed and studied a nonlinear time-fractional mathematical model of the Ebola Virus to understand the outbreak of disease in the community. Their model analysis included both Caputo and Atangana Baleanu fractional derivative operators to solve the solution of the system of fractional differential equations. One of the key findings from their work was that fractional-order derivative showed significant changes and memory effects compared to classical-order derivatives. Farman et al. [33] studied a nonlinear fractional order Ebola virus mathematical model to explore the effects control strategies on the spread of disease in the population. They used Laplace with Adomian Decomposition to solved the fractional differential systems. Their results revealed that, as the order of derivative decreased, the disease died out in the population. Area et al. [30] used both classical and fractional order Ebola epidemic model to fit the real data of Ebola cases reported in Guinea, Liberia and Sierra Leone. In numerical simulations, they found that the fractional-order model gave a better prediction of the disease compared to classical order derivatives. Mathematical studies of fractional order differential equations in disease modeling are also found in [28, 36, 37, 38, 39, 40, 41, 42] and the references therein.

Mathematical modelling, as a powerful tool in quantifying the complex and numerous factors, has widely been developed to explore the transmission dynamics of EVD [9, 10, 11]. One of the emerging areas in biological research is to understand the role of memory effects on the short and long-term dynamics of infectious diseases. Thus, in this study a mathematical model for EVD based on Fractional Calculus is proposed and analyzed. Although this is not the first study to incorporate Fractional Calculus in analyzing EVD transmission (see, for example [30, 34, 43], the proposed model is unique from those in literature in that it also incorporates the direct and indirect disease transmission rates, and effects of cultural beliefs and educational campaigns on funeral and burial practices. Here, EVD transmission rate is being modeled by the mass action incidence which is appropriate when the population is not too large [44]. One of the most commonly performed funeral rituals, which significantly contributes to the spread of Ebola, is the washing and cleaning of dead bodies. Another burial ritual involves relatives of the deceased washing their hands in a common bowl after which they touch the face of the deceased in what is perceived as a 'love touch' that cements unity between the living and ancestral spirits [45]. We assume that the transmission rate of EVD is dependent on the size of the population attending funerals and the burial practices which implies that the contact rate is an increasing function of the population. The mass action incidence is density- dependent since contact rate per infective is proportional to the density of infectious hosts.

Motivated by the above-mentioned works, we derive a fractional-order model for EVD based on the Caputo derivative. The choice of Caputo derivative is also aided by the fact that the Caputo derivative for a given function which is constant is zero. Thus, the Caputo operator computes an ordinary differential equation, followed by a fractional integral to obtain the desired order of fractional derivative [37, 46, 47]. Most importantly, the Caputo fractional derivative allows the use of local initial conditions to be included in the derivation of the model [29, 34, 47, 48].

In Section 2, we present the preliminaries on the Caputo fractional calculus. The proposed model and analytical results are presented in Section 3. In Section 4, the numerical simulations are done to verify the theoretical results presented in the study. Finally, a concluding remark rounds up the paper.

2 Preliminary Results

The basic idea of fractional order derivative was first initiated by Riemann and Liouville, and another by Caputo which is based on the exponential kernel. The main advantage of Caputo fractional order derivative over Riemann-Liouville fractional operator is that: Caputo fractional order derivative provides standard initial conditions which have clear physical interpretation of the problem. Besides, Caputo fractional order derivative is bounded, meaning that the derivative of any constant function is zero. Motivated by the benefits of Caputo fractional operator over the other operators, the proposed model in this study is based on the Caputo fractional derivatives which is an important tool for describing the memory and heredity properties.

2.1 Mathematical concepts of fractional order

In this section we start with mathematical concepts of of Caputo fractional order derivatives which will be used in analysis of proposed Ebola model (see,[28, 49]). The details can be obtained in Appendix A.

3 Materials and Methods

3.1 Description of model and analytical results

Motivated by the works in [9, 10, 11, 30, 43, 34], we are concerned with the impact of educational campaigns on funeral and burial practices. We subdivide the total population of humans $N(t)$ into categories of: susceptible population unaware of the disease fighting means $S(t)$, susceptible population aware of the disease fighting means $E(t)$; infected individuals who are displaying clinical signs of the disease and are infectious $I(t)$, individuals who have recovered from infection $R(t)$, and the deceased population $D(t)$. Let $P(t)$ denote the pathogen population in the environment.

The EVD transmission rate is modeled by the mass action incidence which is appropriate when $N(t)$ is not too large [44]. We assume that the transmission rate is dependent on the size of the population which implies that the contact rate is an increasing function of the population. The mass action incidence is density- dependent since the contact rate per infective is proportional to the density of the infectious host.

The proposed fractional-order derivatives EVD model is given by:

$$\left.\begin{array}{rcl} D^{\alpha}_{t_0}S(t) &=& \Lambda-(\beta_1 I(t)+\beta_2 D(t)+\lambda P(t))S(t)+\phi E(t)-(\mu+\psi)S(t),\\ D^{\alpha}_{t_0}E(t) &=& \psi S(t)-\gamma(\beta_1 I(t)+\beta_2 D(t)+\lambda P(t))E(t)-(\phi+\mu)E(t),\\ D^{\alpha}_{t_0}I(t) &=& (\beta_1 I(t)+\beta_2 D(t)+\lambda P(t))(S(t)+\gamma E(t))-(\mu+\sigma+\delta)I(t),\\ D^{\alpha}_{t_0}R(t) &=& \sigma I(t)-\mu R(t),\\ D^{\alpha}_{t_0}D(t) &=& (\mu+\delta)I(t)-\epsilon D(t),\\ D^{\alpha}_{t_0}P(t) &=& \rho I(t)+\theta D(t)-(\tau+\eta)P(t), \end{array}\right\} \tag{1}$$

where $D^{\alpha}_{t_0}$ denotes the Caputo-fractional calculus and α with $0<\alpha\leq 1$ is the fractional order. The model flow diagram is depicted in Fig. 1.

Additional biological and epidemiological assumptions that govern the model (1) are::

(i) Model (1) exhibits some time dimension problems between left-and right-hand sides of the equations. On the left, the dimension is $(time)^{-\alpha}$, whereas on the right-hand side the dimension is $(time)^{-1}$. To balance the model, the corrected system corresponding to model (1) is as follows:

$$\left.\begin{array}{rcl} D^{\alpha}_{t_0}S(t) &=& \Lambda^{\alpha}-(\beta_1^{\alpha} I(t)+\beta_2^{\alpha} D(t)+\lambda^{\alpha} P(t))S(t)+\phi^{\alpha} E(t)-(\mu^{\alpha}+\psi^{\alpha})S(t),\\ D^{\alpha}_{t_0}E(t) &=& \psi^{\alpha} S(t)-\gamma^{\alpha}(\beta_1^{\alpha} I(t)+\beta_2^{\alpha} D(t)+\lambda^{\alpha} P)E(t)-(\phi^{\alpha}+\mu^{\alpha})E(t),\\ D^{\alpha}_{t_0}I(t) &=& (\beta_1^{\alpha} I(t)+\beta_2^{\alpha} D(t)+\lambda^{\alpha} P(t))(S(t)+\gamma^{\alpha} E(t))-(\mu^{\alpha}+\sigma^{\alpha}+\delta^{\alpha})I(t),\\ D^{\alpha}_{t_0}R(t) &=& \sigma^{\alpha} I(t)-\mu^{\alpha} R(t),\\ D^{\alpha}_{t_0}D(t) &=& (\mu^{\alpha}+\delta^{\alpha})I(t)-\epsilon^{\alpha} D(t),\\ D^{\alpha}_{t_0}P(t) &=& \rho^{\alpha} I(t)+\theta^{\alpha} D(t)-(\tau^{\alpha}+\eta^{\alpha})P(t), \end{array}\right\} \tag{2}$$

(ii) All new recruits are assumed to be susceptible and unaware of the disease and recruited at the rate Λ. Natural mortality occurs at the rate μ. Meanwhile, the susceptible populations are educated at the rate ψ per-day and some educated populations can stop following the preventive measures at the rate ϕ. There is evidence in [50, 51] that Ebola outbreak can last for more than two years which allows the demographic process to take place. Therefore, we have included vital dynamics in our model since the 2014 Ebola outbreak in Guinea.

(iii) Susceptible unaware individuals become aware of the infection through educational campaigns at the rate ψ. Due to memory fading and/or carelessness, susceptible aware individuals become unaware individuals at the rate ϕ:

(iv) Susceptible individuals are assumed to acquire the infection either directly (through contact with either infectious individuals or deceased EVD patients) or, indirectly through contaminated environment. Model parameters β_1, β_2 and λ account for disease transmission when susceptible individuals come into contact with infectious individuals, deceased patients and the environment respectively. Susceptible aware individuals are assumed to have reduced chances of contracting the disease, modeled by $0 < \gamma < 1$, where γ is the disease modification factor that accounts for the impact of educational campaigns on disease transmission.

(v) Infected individuals either recover from infection permanently (at the rate σ) or, succumb to disease-related death at the rate δ. The deceased individual are buried after ϵ^{-1} days. Infectious and deceased EVD patients contaminate the environment at the rates ρ and θ, respectively. The population of pathogens in the environment decreases due to natural decay (at the rate τ) or decontamination (at the rate η).

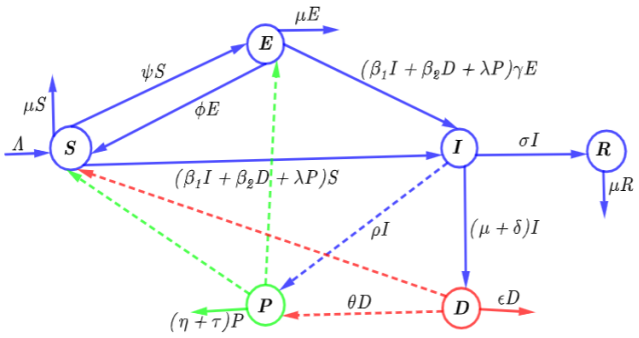

Fig. 1. Flow chart for Ebola virus disease

3.1.1 Non-negativity and boundedness of model solutions

Since model (2) investigate human population, it is important to demonstrate that all model solutions are bounded and positive for all $t \geq 0$. From the computations presented in Appendix B we obtained the following results.

Theorem 3.1. *Model (2) has unique and non-negative solutions which turn into region* Γ_+ *as* $t \to \infty$, *where* Γ_+ *is defined by:* $\Gamma_+ = \left\{ (S(t), E(t), I(t), R(t), D(t), P(t)) \in \mathbb{R}^6_+; S(t) + E(t) + I(t) + R(t) + D(t) + P(t) = N = \frac{\Lambda^\alpha}{\mu^\alpha}, D = \frac{(\mu^\alpha + \delta^\alpha)\Lambda^\alpha}{\mu^\alpha \epsilon^\alpha}, P = \frac{\epsilon^\alpha \rho^\alpha \Lambda^\alpha + \theta^\alpha(\mu^\alpha + \delta^\alpha)\Lambda^\alpha}{\mu^\alpha \epsilon^\alpha(\tau^\alpha + \eta^\alpha)} \right\}$

3.1.2 The basic reproduction number

In this section, we study the basic reproduction number and the existence of a disease-free equilibrium and an endemic equilibrium of the model (2). The model (2) always has a disease-free equilibrium

$$\mathcal{E}^0 = (S^0, E^0, I^0, D^0, P^0, R^0) = (S^0, E^0, 0, 0, 0, 0)$$

, with $S^0 = \frac{\Lambda^\alpha(\phi^\alpha + \mu^\alpha)}{\mu^\alpha(\mu^\alpha + \phi^\alpha + \psi^\alpha)}$, $E^0 = \frac{\Lambda^\alpha \psi^\alpha}{\mu^\alpha(\mu^\alpha + \phi^\alpha + \psi^\alpha)}$, and $S^0 + \gamma^\alpha E^0 = \frac{\Lambda^\alpha(\phi^\alpha + \mu^\alpha + \gamma^\alpha\psi^\alpha)}{\mu^\alpha(\mu^\alpha + \phi^\alpha + \psi^\alpha)}$. By means of the next generation matrix (see, for example, van den Driessche and Watmough [18], one obtains the basic reproduction number of the model (2) as follows:

$$\begin{aligned}\mathcal{R}_0 &= \frac{(S^0 + \gamma^\alpha E^0)\beta_1^\alpha}{(\mu^\alpha + \sigma^\alpha + \delta^\alpha)} + \frac{(S^0 + \gamma^\alpha E^0)(\mu^\alpha + \delta^\alpha)\beta_2^\alpha}{\epsilon^\alpha(\mu^\alpha + \sigma^\alpha + \delta^\alpha)} + \frac{(S^0 + \gamma^\alpha E^0)\theta^\alpha(\mu^\alpha + \delta^\alpha)\lambda^\alpha}{\epsilon^\alpha(\tau^\alpha + \eta^\alpha)(\mu^\alpha + \sigma^\alpha + \delta^\alpha)} \\ &\quad + \frac{(S^0 + \gamma^\alpha E^0)\rho^\alpha\lambda^\alpha}{(\tau^\alpha + \eta^\alpha)(\mu^\alpha + \sigma^\alpha + \delta^\alpha)} \end{aligned} \tag{3}$$

Biologically, the basic reproduction number $\mathcal{R}_0$ represents the average number of new or secondary EVD infections caused by the introduction of an infectious individual into a totally susceptible population. It follows that model (2) has a disease-free equilibrium point $\mathcal{E}^0 = (S^0, E^0, I^0, D^0, P^0, R^0)$ which exists whenever $\mathcal{R}_0 < 1$ and it provides a criterion for the extinction of the disease. In addition to the disease-free equilibrium $\mathcal{E}^0$, the model (2) has a unique endemic equilibrium point $\mathcal{E}^* = (S^*, E^*, I^*, D^*, P^*, R^*)$, which exists whenever $\mathcal{R}_0 > 1$, the EVD infection persists, where:

$$S^* = \frac{\Lambda^\alpha[\gamma^\alpha(\beta_1^\alpha I^* + \beta_2^\alpha D^* + \lambda^\alpha P^*) + (\mu^\alpha + \phi^\alpha)]}{n_1 n_2 - \phi^\alpha\psi^\alpha}, \tag{4}$$

$$E^* = \frac{\Lambda^\alpha\psi^\alpha}{n_1 n_2 - \phi^\alpha\psi^\alpha}, \tag{5}$$

with $n_1 = [(\beta_1^\alpha I^* + \beta_2^\alpha D^* + \lambda^\alpha P^*) + (\mu^\alpha + \psi^\alpha)]$ and $n_2 = [\gamma^\alpha(\beta_1^\alpha I^* + \beta_2^\alpha D^* + \lambda^\alpha P^*) + (\mu^\alpha + \phi^\alpha)]$

$$\begin{aligned} D^* = \frac{(\mu^\alpha + \delta^\alpha)I^*}{\epsilon^\alpha}, \qquad R^* = \frac{\rho^\alpha I^*}{\mu^\alpha}, \qquad \text{and} \\ P^* = \frac{\rho^\alpha I^*}{(\tau^\alpha + \eta^\alpha)} + \frac{\theta^\alpha(\mu^\alpha + \delta^\alpha)I^*}{\epsilon^\alpha(\tau^\alpha + \eta^\alpha)}. \end{aligned} \tag{6}$$

Substituting equation (6) into the third equation in (2), gives:

$$\begin{aligned} &\beta_1^\alpha I^*(S^* + \gamma^\alpha E^*) + \frac{\beta_2^\alpha(\mu^\alpha + \delta^\alpha)I^*(S^* + \gamma^\alpha E^*)}{\epsilon^\alpha} + \frac{\lambda^\alpha\rho^\alpha I^*(S^* + \gamma^\alpha E^*)}{(\tau^\alpha + \eta^\alpha)} \\ &+ \frac{\lambda^\alpha\theta^\alpha(\mu^\alpha + \delta^\alpha)I^*(S^* + \gamma^\alpha E^*)}{\epsilon^\alpha(\tau^\alpha + \eta^\alpha)} - (\mu^\alpha + \sigma^\alpha + \delta^\alpha)I^* = 0. \end{aligned} \tag{7}$$

From (31), we have:

$$\begin{aligned} &\left(\frac{\beta_1^\alpha I^*(S^* + \gamma^\alpha E^*)}{(\mu^\alpha + \sigma^\alpha + \delta^\alpha)} + \frac{\beta_2^\alpha(\mu^\alpha + \delta^\alpha)I^*(S^* + \gamma^\alpha E^*)}{\epsilon^\alpha(\mu^\alpha + \sigma^\alpha + \delta^\alpha)} + \frac{\lambda^\alpha\rho^\alpha I^*(S^* + \gamma^\alpha E^*)}{(\tau^\alpha + \eta^\alpha)(\mu^\alpha + \sigma^\alpha + \delta^\alpha)}\right. \\ &\left. + \frac{\lambda^\alpha\theta^\alpha(\mu^\alpha + \delta^\alpha)I^*(S^* + \gamma^\alpha E^*)}{\epsilon^\alpha(\tau^\alpha + \eta^\alpha)(\mu^\alpha + \sigma^\alpha + \delta^\alpha)} - 1\right) \times (\mu^\alpha + \sigma^\alpha + \delta^\alpha)I^* = 0. \end{aligned}$$

It follows that:

$$I^* = 0, \qquad \text{or}$$

$$(S^* + \gamma^\alpha E^*) = \frac{\epsilon^\alpha(\tau^\alpha + \eta^\alpha)(\mu^\alpha + \sigma^\alpha + \delta^\alpha)}{r}, \tag{8}$$

with $r = \beta_1^\alpha \epsilon^\alpha(\tau^\alpha + \eta^\alpha) + \beta_2^\alpha \eta^\alpha(\mu^\alpha + \delta^\alpha) + \lambda^\alpha \epsilon^\alpha \rho^\alpha + \theta^\alpha \lambda^\alpha(\mu^\alpha + \delta^\alpha)$. Substituting the value of S^* and E^* into (32), yields:

$$g(I^*) = A(I^*)^2 + BI^* + C, \tag{9}$$

where:

$$\begin{aligned}
A &= \epsilon^\alpha(\tau^\alpha + \eta^\alpha)(\mu^\alpha + \sigma^\alpha + \delta^\alpha)\gamma^\alpha \lambda^{2\alpha} \times \left[\frac{\rho^\alpha}{(\tau^\alpha + \eta^\alpha)} + \frac{\theta^\alpha(\mu^\alpha + \delta^\alpha)}{\epsilon^\alpha(\tau^\alpha + \eta^\alpha)}\right]^2 \\
&\quad + \epsilon^\alpha(\tau^\alpha + \eta^\alpha)(\mu^\alpha + \sigma^\alpha + \delta^\alpha)\gamma^\alpha \beta_1^{c\alpha} + \frac{(\tau^\alpha + \eta^\alpha)(\mu^\alpha + \sigma^\alpha + \delta^\alpha)\gamma^\alpha \beta_2^{2\alpha}(\mu^\alpha + \delta^\alpha)^2}{\epsilon^\alpha} \\
&\quad + 2(\tau^\alpha + \eta^\alpha)(\mu^\alpha + \sigma^\alpha + \delta^\alpha)(\mu^\alpha + \delta^\alpha)\gamma^\alpha \beta_1^\alpha \beta_2^\alpha + 2\gamma^\alpha \beta_1^\alpha \lambda^\alpha(\mu^\alpha + \sigma^\alpha + \delta^\alpha)(\rho^\alpha \epsilon^\alpha + \theta^\alpha(\mu^\alpha \\
&\quad + \delta^\alpha)) + 2\gamma^\alpha \beta_2^\alpha \lambda^\alpha(\mu^\alpha + \sigma^\alpha + \delta^\alpha)(\mu^\alpha + \delta^\alpha \times \left(\rho^\alpha + \frac{\theta^\alpha(\mu^\alpha + \delta^\alpha)}{\epsilon^\alpha}\right), \\
B &= \left[\gamma^\alpha \mu^\alpha + (\mu^\alpha + \phi^\alpha + \gamma^\alpha \psi^\alpha) - \frac{M}{\epsilon^\alpha(\tau^\alpha + \eta^\alpha)(\mu^\alpha + \sigma^\alpha + \delta^\alpha)}\right] \\
&\quad \times (\mu^\alpha + \sigma^\alpha + \delta^\alpha)[\beta_1^\alpha \epsilon^\alpha(\tau^\alpha + \eta^\alpha) + \beta_2^\alpha(\tau^\alpha + \eta^\alpha)(\mu^\alpha + \delta^\alpha) + \lambda^\alpha \epsilon^\alpha \rho^\alpha + \theta^\alpha \lambda^\alpha(\mu^\alpha + \delta^\alpha)], \\
C &= \epsilon^\alpha \mu^\alpha(\tau^\alpha + \eta^\alpha)(\mu^\alpha + \sigma^\alpha + \delta^\alpha)(\mu^\alpha + \phi^\alpha + \psi^\alpha)\left[1 - \mathcal{R}_0\right], where, \\
M &= \gamma^\alpha \Lambda^\alpha(\beta_1^\alpha \epsilon^\alpha(\tau^\alpha + \eta^\alpha) + \beta_2^\alpha(\tau^\alpha + \eta^\alpha)(\mu^\alpha + \delta^\alpha) + \lambda^\alpha \epsilon^\alpha \rho^\alpha + \theta^\alpha \lambda^\alpha(\mu^\alpha + \delta^\alpha)).
\end{aligned}$$

Using the fact that all parameters in the model (2) are positive for $t \geq 0$, it follows from Equation (9) that $A > 0$. Furthermore, $C > 0$ when $\mathcal{R}_0 < 1$. Therefore, the number of possible positive real roots of the polynomial (9) hinges on the signs of B and C. By applying the Descartes rule of signs on the polynomial (9) $g(I^*) = 0$, given in (9), we list the various possibilities for the roots of $g(I^*)$ in Table 1:

Table. 1. Number of various possibilities for the roots of $g(I^*)$ for $\mathcal{R}_0 < 1$ and $\mathcal{R}_0 > 1$.

Case	A	B	C	$\mathcal{R}_0$	No. of sign changes	No. of various possibilities for the roots
1	+	+	+	$\mathcal{R}_0 < 1$	0	0
2	+	+	-	$\mathcal{R}_0 > 1$	1	1
3	+	-	+	$\mathcal{R}_0 < 1$	2	0,2
4	+	-	-	$\mathcal{R}_0 > 1$	1	1

Based on the various possibilities in Table 1, we have the following results:

Theorem 3.2. *The model (2) admits that:*

(i) *a unique endemic equilibrium $\mathcal{E}^*$ if $\mathcal{R}_0 > 1$ and Cases 2 and 4 are satisfied,*

(ii) *more than one endemic equilibrium if $\mathcal{R}_0 < 1$ part of Case 3 holds,*

(iii) *no endemic equilibrium if $\mathcal{R}_0 < 1$, and Cases 1 and part of Case 3 are satisfied.*

3.1.3 Global stability

In this section, we are concerned with the global stability of the disease-free equilibrium $\mathcal{E}^0 = (S^0, E^0, 0, 0, 0, 0)$ and the endemic equilibrium $\mathcal{E}^* = (S^*, E^*, I^*, D^*, P^*, R^*)$ of the model (2). To investigate the global stability of the model steady states we will construct appropriate Lyapunov functionals. Since the recovered/removed

population does not contribute to the generation of secondary infections one can ignore that fourth equation of model (2) when examining the global stability and consider the following reduced system:

$$\left.\begin{array}{rcl} D^{\alpha}_{t_0}S(t) &=& \Lambda^{\alpha} - (\beta_1^{\alpha}I(t) + \beta_2^{\alpha}D(t) + \lambda^{\alpha}P(t))S(t) + \phi^{\alpha}E(t) - m_1S(t), \\ D^{\alpha}_{t_0}E(t) &=& \psi^{\alpha}S(t) - \gamma^{\alpha}(\beta_1^{\alpha}I(t) + \beta_2^{\alpha}D(t) + \lambda^{\alpha}P)E(t) - m_2E(t), \\ D^{\alpha}_{t_0}I(t) &=& [(\beta_1^{\alpha}I(t) + \beta_2^{\alpha}D(t) + \lambda^{\alpha}P(t))S(t) + \gamma^{\alpha}(\beta_1^{\alpha}I(t) + \beta_2^{\alpha}D(t) + \lambda^{\alpha}P)E(t)] \\ && -m_3I(t), \\ D^{\alpha}_{t_0}D(t) &=& m_4I(t) - \epsilon^{\alpha}D(t), \\ D^{\alpha}_{t_0}P(t) &=& \rho^{\alpha}I(t) + \theta^{\alpha}D(t) - m_5P(t), \end{array}\right\} \tag{10}$$

with $m_1 = (\mu^{\alpha} + \psi^{\alpha})$, $m_2 = (\phi^{\alpha} + \mu^{\alpha})$, $m_3 = (\mu^{\alpha} + \sigma^{\alpha} + \delta^{\alpha})$, $m_4 = (\mu^{\alpha} + \delta^{\alpha})$, and $m_5 = (\tau^{\alpha} + \eta^{\alpha})$.

To investigate the global stability of the disease-free equilibrium point $\mathcal{E}^0$ and the endemic equilibrium $\mathcal{E}^*$ of model (10), we utilize the Lyapunov function whose origin is ecology but was extended to epidemiology models and then effectively applied to a variety of compartment models (see for example [56]).

We begin by introducing the following definition of positive definite function (see, [57]) that we use to develop the Lyapunov's function.

Definition 1. *(***Positive definite function** *[57]) Let $\mathcal{V}(t) : \mathbb{R}^n \longrightarrow \mathbb{R}$ be a continuously differentiable real valued function. Then $\mathcal{V}(t)$ is said to be positive definite function if:*

1. *$\mathcal{V}(t^0) = 0$, and:*
2. *$\mathcal{V}(t) > 0$ for all $t \neq t^0$*

Theorem 3.3. *(Fractional La-Salle invariance principle [28, 49]). Let $x^* \in \Gamma \subset \mathbb{R}^n$ be an equilibrium point for the non-autonomous fractional order system $D^{\alpha}_{t_0} = f(t, x)$. Let $L : [0, \infty) \times \Gamma \to \mathbb{R}$ be a continuously differentiable function such that:*

$$\mathcal{M}_1(x) \leq L(t, x(t)) \leq \mathcal{M}_2(x)$$

and:

$$D^{\alpha}_{t_0}L(t, x(t)) \leq -\mathcal{M}_3(x),$$

for all $\alpha \in (0, 1)$ and all $x \in \Gamma$, where $\mathcal{M}_1(x)$, $\mathcal{M}_2(x)$ and $\mathcal{M}_3(x)$ are continuous positive definite functions on Γ. Then the equilibrium point x^* is uniformly asymptotically stable.

Now using Theorem (3.3) we will show that the disease-free equilibrium $\mathcal{E}^0$ and the endemic equilibrium point $\mathcal{E}^*$ of system (10) are globally asymptotically stable

Theorem 3.4. *For $\alpha \in (0, 1]$, the disease-free equilibrium $\mathcal{E}^0$ of system (10) is globally asymptotically stable whenever $\mathcal{R}_0 \leq 1$.*

Proof. Consider the following appropriate Lyapunov function:

$$\mathcal{V}(t) = \left(\frac{\beta_1^{\alpha}}{m_3} + \frac{\beta_2^{\alpha}m_4}{\epsilon^{\alpha}m_3} + \frac{\theta^{\alpha}\lambda^{\alpha}m_4}{\epsilon^{\alpha}m_5m_3} + \frac{\lambda^{\alpha}\rho^{\alpha}}{m_5m_3}\right)I(t) + \left(\frac{\beta_2^{\alpha}}{\epsilon^{\alpha}} + \frac{\theta^{\alpha}\lambda^{\alpha}}{\epsilon^{\alpha}m_5}\right)D(t) + \frac{\lambda^{\alpha}}{m_5}P(t).$$

Then the time fractional order derivative of $\mathcal{V}(t)$ along solutions of model (10):

$$\begin{aligned} D^{\alpha}_{t_0}\mathcal{V}(t) &= \left(\frac{\beta_1^{\alpha}}{m_3} + \frac{\beta_2^{\alpha}m_4}{\epsilon^{\alpha}m_3} + \frac{\theta^{\alpha}\lambda^{\alpha}m_4}{\epsilon^{\alpha}m_5m_3} + \frac{\lambda^{\alpha}\rho^{\alpha}}{m_5m_3}\right) \times \left(\beta_1^{\alpha}I(t) + \beta_2^{\alpha}D(t) + \lambda^{\alpha}P(t)\right) \\ &\quad \times \left(S(t) + \gamma^{\alpha}E(t)\right) - \left(\beta_1^{\alpha}I(t) + \beta_2^{\alpha}D(t) + \lambda^{\alpha}P(t)\right) \end{aligned}$$

$$= \left[\left(\frac{\beta_1^\alpha}{m_3}+\frac{\beta_2^\alpha m_4}{\epsilon^\alpha m_3}+\frac{\theta^\alpha\lambda^\alpha m_4}{\epsilon^\alpha m_5 m_3}+\frac{\lambda^\alpha\rho^\alpha}{m_5 m_3}\right)\times\left(S(t)+\gamma^\alpha E(t)\right)-1\right] \times\left[\beta_1^\alpha I(t)+\beta_2^\alpha D(t)+\lambda^\alpha P(t)\right].$$

Since $S^0 \le S(t), E^0 \le E(t), \left(S^0+\gamma^\alpha E^0 = \frac{\Lambda^\alpha(\phi^\alpha+\mu^\alpha+\gamma^\alpha\psi^\alpha)}{\mu^\alpha(\mu^\alpha+\phi^\alpha+\psi^\alpha)}\right)$ for $t \ge 0$ we have:

$$\begin{aligned} D_{t_0}^\alpha \mathcal{V}(t) &\le \left[\left(\frac{\beta_1^\alpha}{m_3}+\frac{\beta_2^\alpha m_4}{\epsilon^\alpha m_3}+\frac{\theta^\alpha\lambda^\alpha m_4}{\epsilon^\alpha m_5 m_3}+\frac{\lambda^\alpha\rho^\alpha}{m_5 m_3}\right)\times\left(\frac{\Lambda^\alpha(\phi^\alpha+\mu^\alpha+\gamma^\alpha\psi^\alpha)}{\mu^\alpha(\mu^\alpha+\phi^\alpha+\psi^\alpha)}\right)-1\right] \\ &\quad\times\left[\beta_1^\alpha I(t)+\beta_2^\alpha D(t)+\lambda^\alpha P(t)\right] \\ &= \left[\mathcal{R}_0-1\right]\left[\beta_1^\alpha I(t)+\beta_2^\alpha D(t)+\lambda^\alpha P(t)\right]. \end{aligned} \tag{11}$$

Therefore, $D_{t_0}^\alpha \mathcal{V}(t) < 0$ holds if $\mathcal{R}_0 < 1$. Furthermore if $\mathcal{R}_0 = 1$, $D_{t_0}^\alpha \mathcal{V}(t) = 0$ if and only if $S(t) = S^0$, $E(t) = E^0$, $I(t) = D(t) = P(t) = 0$. Thus, the largest compact invariant set in $U_1 = \left\{(S^0, E^0, 0, 0, 0) \in \Gamma : D_{t_0}^\alpha \mathcal{V}(t) = 0\right\}$ is a singleton set containing the disease-free equilibrium $\mathcal{E}^0$. Therefore, by Theorem (3.3), we conclude that the disease-free equilibrium is globally asymptotically stable in Γ. □

Next, we investigate the global stability of the endemic equilibrium point $\mathcal{E}^*$ of model (10) when $\mathcal{R}_0 > 1$.

Theorem 3.5. *For $\alpha \in (0, 1]$, whenever $\mathcal{R}_0 > 1$, then model (10) has a globally asymptotically stable endemic equilibrium point $\mathcal{E}^*$.*

Proof. Let us consider the following appropriate Lyapunov function:

$$\begin{aligned} \mathcal{W}(t) &= \left\{S(t)-S^*-S^*\ln\left(\frac{S(t)}{S^*}\right)\right\}+\left\{E(t)-E^*-E^*\ln\left(\frac{E(t)}{E^*}\right)\right\} \\ &\quad+\left\{I(t)-I^*-I^*\ln\left(\frac{I(t)}{I^*}\right)\right\}+\frac{[\beta_2^\alpha D^*(\rho^\alpha I^*+\theta^\alpha D^*)+\lambda^\alpha P^*\theta^\alpha D^*]\,(S^*+\gamma^\alpha E^*)}{m_4 I^*[\rho^\alpha I^*+\theta^\alpha D^*]} \\ &\quad\times\left\{D(t)-D^*-D^*\ln\left(\frac{D(t)}{D^*}\right)\right\}+\frac{\lambda^\alpha P^*(S^*+\gamma^\alpha E^*)}{[\rho^\alpha I^*+\theta^\alpha D^*]} \\ &\quad\times\left\{P(t)-P^*-P^*\ln\left(\frac{P(t)}{P^*}\right)\right\} \end{aligned} \tag{12}$$

The time fractional order derivatives of $\mathcal{W}(t)$ are given by:

$$\begin{aligned} D_{t_0}^\alpha \mathcal{W}(t) &= \left(1-\frac{S^*}{S(t)}\right)D_{t_0}^\alpha S(t)+\left(1-\frac{E^*}{E(t)}\right)D_{t_0}^\alpha E(t)+\left(1-\frac{I^*}{I(t)}\right)D_{t_0}^\alpha I(t) \\ &\quad+\frac{[\beta_2^\alpha D^*(\rho^\alpha I^*+\theta^\alpha D^*)+\lambda^\alpha P^*\theta^\alpha D^*]}{m_4 I^*[\rho^\alpha I^*+\theta^\alpha D^*]}\times(S^*+\gamma^\alpha E^*)\left(1-\frac{D^*}{D(t)}\right)D_{t_0}^\alpha D(t) \\ &\quad+\frac{\lambda^\alpha P^*(S^*+\gamma^\alpha E^*)}{[\rho^\alpha I^*+\theta^\alpha D^*]}\left(1-\frac{P^*}{P(t)}\right)D_{t_0}^\alpha P(t). \end{aligned} \tag{13}$$

Substituting the appropriate derivatives according to equations (10), we have:

$$D_{t_0}^\alpha \mathcal{W}(t) = \left\{1-\frac{S^*}{S(t)}\right\}\left\{\psi^\alpha S(t)-\gamma^\alpha(\beta_1^\alpha I(t)+\beta_2^\alpha D(t)+\lambda^\alpha P)E(t)-(\phi^\alpha+\mu^\alpha)E(t)\right\}$$

$$
\begin{aligned}
&+\Big\{1-\frac{E^*}{E(t)}\Big\}\Big\{\psi^\alpha S(t)-\phi^\alpha E(t)-\mu^\alpha E-\gamma^\alpha\beta_1^\alpha I(t)E(t)-\gamma^\alpha\beta_2^\alpha D_1(t)E(t)\Big\}\\
&+\Big\{1-\frac{I^*}{I(t)}\Big\}\Big\{[(\beta_1^\alpha I(t)+\beta_2^\alpha D(t)+\lambda^\alpha P(t))S(t)+\gamma^\alpha(\beta_1^\alpha I(t)+\beta_2^\alpha D(t)\\
&+\lambda^\alpha P)E(t)]\\
&-(\mu^\alpha+\sigma^\alpha+\delta^\alpha)I(t)\Big\}+\frac{[\beta_2^\alpha D^*(\rho^\alpha I^*+\theta^\alpha D^*)+\lambda^\alpha P^*\theta^\alpha D^*]\,(S^*+\gamma^\alpha E^*)}{m_4 I^*[\rho^\alpha I^*+\theta^\alpha D^*]}\\
&\times\Big\{1-\frac{D^*}{D(t)}\Big\}\Big\{(\mu^\alpha+\delta^\alpha)I(t)-\epsilon^\alpha D(t)\Big\}+\frac{\lambda^\alpha P^*(S^*+\gamma^\alpha E^*)}{[\rho^\alpha I^*+\theta^\alpha D^*]}\Big\{1-\frac{P^*}{P(t)}\Big\}\\
&\times\Big\{\rho^\alpha I(t)+\theta^\alpha D(t)-(\tau^\alpha+\eta^\alpha)P(t)\Big\}. \qquad (14)
\end{aligned}
$$

At endemic equilibrium, we have:

$$
\begin{cases}
\Lambda^\alpha &= \beta_1^\alpha I^*S^*+\beta_2^\alpha D^*S^*+\lambda^\alpha P^*S^*+\mu^\alpha S^*+\psi^\alpha S^*-\phi^\alpha E^*,\\
\psi^\alpha S^* &= \phi^\alpha E^*+\mu^\alpha E^*+\gamma^\alpha\beta_1^\alpha I^*E(t)+\gamma^\alpha\beta_2^\alpha D^*E^*+\gamma^\alpha\lambda^\alpha P^*E^*,\\
(\mu^\alpha+\sigma^\alpha+\delta^\alpha)I^* &= \beta_1^\alpha I^*S^*+\beta_2^\alpha D^*S^*+\lambda^\alpha P^*S^*+\gamma^\alpha\beta_1^\alpha I^*E^*+\gamma^\alpha\beta_2^\alpha D^*E^*\\
&\quad +\gamma^\alpha\lambda^\alpha P^*E^*,\\
\epsilon^\alpha D^* &= (\mu^\alpha+\delta^\alpha)I^*,\\
(\tau^\alpha+\eta^\alpha)P^* &= \rho^\alpha I^*+\theta^\alpha D^*.
\end{cases} \qquad (15)
$$

Using the above constants at endemic equilibrium, we have:

$$
\begin{aligned}
D_{t_0}^\alpha\mathcal{W}(t) &= (\mu^\alpha+\beta_1^\alpha I^*)S^*\left\{2-\frac{S(t)}{S^*}-\frac{S^*}{S(t)}\right\}+(\mu^\alpha+\gamma^\alpha\beta_1^\alpha I^*)E^*\Big\{3-\frac{S(t)}{S^*}.\frac{E^*}{E(t)}\\
&\quad-\frac{S^*}{S(t)}-\frac{E(t)}{E^*}\Big\}+\phi^\alpha E^*\left\{2-\frac{S(t)}{S^*}.\frac{E^*}{E(t)}-\frac{S^*}{S(t)}.\frac{E(t)}{E^*}\right\}\\
&\quad+\frac{\lambda^\alpha P^*S^*\rho^\alpha I^*}{(\rho^\alpha I^*+\theta^\alpha D^*)}\Big\{3-\frac{S^*}{S(t)}-\frac{I(t)}{I^*}.\frac{P^*}{P(t)}-\frac{P(t)}{P^*}.\frac{I^*}{I(t)}.\frac{S(t)}{S^*}\Big\}\\
&\quad+\frac{\gamma^\alpha\lambda^\alpha P^*E^*\rho^\alpha I^*}{(\rho^\alpha I^*+\theta^\alpha D^*)}\Big\{4-\frac{S^*}{S(t)}-\frac{I(t)}{I^*}.\frac{P^*}{P(t)}-\frac{S(t)}{S^*}.\frac{E^*}{E(t)}-\frac{P(t)}{P^*}.\frac{I^*}{I(t)}.\frac{E(t)}{E^*}\Big\}\\
&\quad+\frac{\lambda^\alpha P^*S^*\theta^\alpha D^*}{(\rho^\alpha I^*+\theta^\alpha D^*)}\Big\{4-\frac{S^*}{S(t)}-\frac{I(t)}{I^*}.\frac{D^*}{D(t)}-\frac{D(t)}{D^*}.\frac{P^*}{P(t)}-\frac{P(t)}{P^*}.\frac{I^*}{I(t)}.\frac{S(t)}{S^*}\Big\}\\
&\quad+\frac{\gamma^\alpha\lambda^\alpha P^*E^*\theta^\alpha D^*}{(\rho^\alpha I^*+\theta^\alpha D^*)}\Big\{5-\frac{S^*}{S(t)}-\frac{I(t)}{I^*}.\frac{D^*}{D(t)}-\frac{D(t)}{D^*}.\frac{P^*}{P(t)}-\frac{S(t)}{S^*}\frac{E^*}{E(t)}\\
&\quad-\frac{P(t)}{P^*}.\frac{I^*}{I(t)}.\frac{E(t)}{E^*}\Big\}+\beta_2^\alpha S^*D^*\Big\{3-\frac{S^*}{S(t)}-\frac{I(t)}{I^*}.\frac{D^*}{D(t)}-\frac{D(t)}{D^*}.\frac{I^*}{I(t)}.\frac{S(t)}{S^*}\Big\}\\
&\quad+\gamma^\alpha\beta_2^\alpha E^*D^*\Big\{4-\frac{S^*}{S(t)}-\frac{S(t)}{S^*}.\frac{E^*}{E(t)}-\frac{I(t)}{I^*}.\frac{D^*}{D(t)}-\frac{D(t)}{D^*}.\frac{I^*}{I(t)}.\frac{E(t)}{E^*}\Big\}. \qquad (16)
\end{aligned}
$$

By the property that the arithmetic mean is greater than or equal to the geometric mean:

$$
2\le\frac{S(t)}{S^*}+\frac{S^*}{S(t)},\quad 2\le\frac{S(t)}{S^*}.\frac{E^*}{E(t)}+\frac{S^*}{S(t)}.\frac{E(t)}{E^*},\quad 3\le\frac{S(t)}{S^*}.\frac{E^*}{E(t)}+\frac{S^*}{S(t)}+\frac{E(t)}{E^*},
$$

$$
3\le\frac{S^*}{S(t)}+\frac{I(t)}{I^*}.\frac{P^*}{P(t)}+\frac{P(t)}{P^*}.\frac{I^*}{I(t)}.\frac{S(t)}{S^*},
$$

$$
4\le\frac{S^*}{S(t)}+\frac{I(t)}{I^*}.\frac{P^*}{P(t)}+\frac{S(t)}{S^*}.\frac{E^*}{E(t)}+\frac{P(t)}{P^*}.\frac{I^*}{I(t)}.\frac{E(t)}{E^*},
$$

$$
4\le\frac{S^*}{S(t)}+\frac{I(t)}{I^*}.\frac{D^*}{D(t)}+\frac{D(t)}{D^*}.\frac{P^*}{P(t)}+\frac{P(t)}{P^*}.\frac{I^*}{I(t)}.\frac{S(t)}{S^*},
$$

$$5 \leq \frac{S^*}{S(t)} + \frac{I(t)}{I^*}.\frac{D^*}{D(t)} + \frac{D(t)}{D^*}.\frac{P^*}{P(t)} + \frac{S(t)}{S^*}\frac{E^*}{E(t)} + \frac{P(t)}{P^*}.\frac{I^*}{I(t)}.\frac{E(t)}{E^*},$$

$$3 \leq \frac{S^*}{S(t)} + \frac{I(t)}{I^*}.\frac{D^*}{D(t)} + \frac{D(t)}{D^*}.\frac{I^*}{I(t)}.\frac{S(t)}{S^*},$$

$$4 \leq \frac{S^*}{S(t)} + \frac{S(t)}{S^*}.\frac{E^*}{E(t)} + \frac{I(t)}{I^*}.\frac{D^*}{D(t)} + \frac{D(t)}{D^*}.\frac{I^*}{I(t)}.\frac{E(t)}{E^*},$$

for all $S(t) > 0$, $E(t) > 0$, $I(t) > 0$, $D(t) > 0$ and $P(t) > 0$, because the arithmetic mean is greater than or equal to the geometric mean. Hence $\mathcal{W}(t) \leq 0$ and consequently, $D^{\alpha}_{t_0}\mathcal{W}(t) \leq 0$. Moreover, the largest compact invariant set in $U_2 = \{(S^*, E^*, I^*, D^*, P^*) \in \Gamma : D^{\alpha}_{t_0}\mathcal{W}(t) = 0\}$ is a singleton set containing the endemic equilibrium $\mathcal{E}^*$, where $S(t) \equiv S^*$, $E(t) \equiv E^*$, $I(t) \equiv I^*$, $D(t) \equiv D^*$, and $P(t) \equiv P^*$. Using Theorem (3.3), we conclude that the endemic equilibrium point $\mathcal{E}^*$ is globally asymptotically stable if $\mathcal{R}_0 > 1$. □

4 Numerical Simulations and Discussions

In this section, we performed the numerical simulations of the model (2) to justify the analytical results. Most of the parameter values which are not available in literature have been estimated within the reasonable realistic situation, the cumulative number of EVD monthly cases from March to August of the 2014 Ebola outbreak in Guinea was utilized (see [9]). We performed the numerical simulations using fractional Adam-Bashforth-Moulton scheme [47] as illustrated in equation (17):

For any differential equation:

$$D^{\alpha}_{t_0}x(t) = g(t, x(t)), \quad 0 \leq t \leq T, \tag{17}$$

with the following initial conditions:

$$x^i(0) = x^i_0, \quad i = 0, 1, 2, 3, ...[\alpha] - 1. \tag{18}$$

Operating by the fractional integral operator on equation (17) we obtain the solution $x(t)$ by solving equation (19):

$$x(t) = \sum_{i=0}^{[\alpha]-1} \frac{x^i_0}{i!}t^i + \frac{1}{\Gamma(\alpha)}\int_0^t (t-\tau)^{\alpha-1}g(\tau, x(\tau))d\tau. \tag{19}$$

Diethelm [58] used the predictor-corrector scheme based on the Adam-Bashforth-Moulton algorithm to numerically solve equation (19). Setting $h = \frac{T}{N}$, $t_n = nh$, and $n = 0, 1, 2, 3, ..N \in \mathbb{Z}^+$, we discretized equation (19) as a fractional variant of the one step Adam-Bashforth-Moulton scheme as shown in equation (20):

$$\begin{aligned} x_h(t_{n+1}) \quad = \quad & \sum_{i=0}^{|\alpha|-1} \frac{x^i_0}{i!}t^i_{n+1} + \frac{h^{\alpha}}{\Gamma(\alpha+2)}\sum_{q=0}^{n} a_{q,n+1}g(t_q, x_q) \\ & + \frac{h^{\alpha}}{\Gamma(\alpha+2)}g(t_{n+1}, x^p_{n+1}), \end{aligned} \tag{20}$$

where: $a_{q,n+1} = \begin{cases} n^{\alpha+1} - (n-\alpha)(n+\alpha)^{\alpha}, & q = 0, \\ (n-q+2)^{\alpha+1} + (n-q)^{\alpha+1} - 2(n-q+1)^{\alpha+1}, & 1 \leq q \leq n, \\ 1, & q = n+1, \end{cases}$

and the predicted value $x^p_h(t_{n+1})$ is determined by:

$$x_h(t_{n+1}) = \sum_{i=0}^{|\alpha|-1} \frac{x^i_0}{i!}t^i_{n+1} + \frac{1}{\Gamma(\alpha)}\sum_{q=0}^{n} b_{q,n+1}g(t_q, x_h(t_q)), \tag{21}$$

with:

$$b_{q,n+1} = \frac{h^\alpha}{\alpha}((n+1-q)^\alpha - (n-q)^\alpha. \tag{22}$$

The error estimate is:

$$\max_{0\le q\le k} |x(t_q) - x_h(t_q)| = O(h^p), \tag{23}$$

with $k \in \mathbb{N}$ and $p = \min(2, 1+\alpha)$.

4.1 Application of Adam-Bashforth-Moulton Scheme to the proposed model

Most of the fractional order derivatives $\alpha \in (0,1)$ that describe the real-world problems are highly complicated and difficult to obtain its numerical approximations due to the existence of their non-local in nature compared to the integer order derivatives. Adam-Bashforth-Moulton scheme have been recognized as a powerful numerical scheme to solve nonlinear fractional order problems due to its stability compared to other methods. Therefore, in this section we utilize the Adam-Bashforth-Moulton scheme to numerically solve the nonlinear fractional model (2). In the view to the generalized Adam-Bashforth-Moulton scheme, the proposed model (2) has the following form:

$$\left.\begin{aligned}
S(t_{n+1}) &= S_0 + \frac{h^\alpha}{\Gamma(\alpha+2)}\big(\Lambda^\alpha - (\beta_1^\alpha I^p(t_{n+1}) + \beta_2^\alpha D^p(t_{n+1}) + \lambda^\alpha P^p(t_{n+1}))S^p(t_{n+1}) \\
&\quad +\phi^\alpha E^p(t_{n+1}) - m_1 S^p(t_{n+1})\big) \\
&\quad + \frac{h^\alpha}{\Gamma(\alpha+2)}\sum_{q=0}^{n} a_{q,n+1}\big(\Lambda^\alpha - (\beta_1^\alpha I(t_q) + \beta_2^\alpha D(t_q) + \lambda^\alpha P(t_q))S(t_q) \\
&\quad +\phi^\alpha E(t_q) - m_1 S(t_q)\big), \\
E(t_{n+1}) &= E_0 + \frac{h^\alpha}{\Gamma(\alpha+2)}\big(\psi^\alpha S^p(t_{n+1}) - \gamma^\alpha(\beta_1^\alpha I^p(t_{n+1}) + \beta_2^\alpha D^p(t_{n+1}) \\
&\quad +\lambda^\alpha P^p(t_{n+1}))E^p(t_{n+1}) - m_2 E^p(t_{n+1})\big) \\
&\quad + \frac{h^\alpha}{\Gamma(\alpha+2)}\sum_{q=0}^{n} a_{q,n+1}\big(\psi^\alpha S(t_q) - \gamma^\alpha(\beta_1^\alpha I(t_q) + \beta_2^\alpha D(t_q) \\
&\quad +\lambda^\alpha P(t_q))E(t_q) - m_2 E(t_q)\big), \\
I(t_{n+1}) &= I_0 + \frac{h^\alpha}{\Gamma(\alpha+2)}\big([(\beta_1^\alpha I^p(t_{n+1}) + \beta_2^\alpha D^p(t_{n+1}) + \lambda^\alpha P^p(t_{n+1}))S^p(t_{n+1}) \\
&\quad +\gamma^\alpha(\beta_1^\alpha I^p(t_{n+1}) + \beta_2^\alpha D^p(t_{n+1}) + \lambda^\alpha P^p(t_{n+1}))E^p(t_{n+1})] - m_3 I^p(t_{n+1})\big) \\
&\quad + \frac{h^\alpha}{\Gamma(\alpha+2)}\sum_{q=0}^{n} a_{q,n+1}\big([(\beta_1^\alpha I(t_q) + \beta_2^\alpha D(t_q) + \lambda^\alpha P(t_q))S(t_q) \\
&\quad +\gamma^\alpha(\beta_1^\alpha I(t_q) + \beta_2^\alpha D(t_q) + \lambda^\alpha P(t_q))E(t_q)] - m_3 I(t_q)\big) \\
R(t_{n+1}) &= R_0 + \frac{h^\alpha}{\Gamma(\alpha+2)}\big(\sigma^\alpha I^p(t_{n+1}) - \mu^\alpha R^p(t_{n+1})\big) \\
&\quad + \frac{h^\alpha}{\Gamma(\alpha+2)}\sum_{q=0}^{n} a_{q,n+1}\big(\sigma^\alpha I(t_q) - \mu^\alpha R(t_q)\big) \\
D(t_{n+1}) &= D_0 + \frac{h^\alpha}{\Gamma(\alpha+2)}\big(m_4 I^p(t_{n+1}) - \epsilon^\alpha D^p(t_{n+1})\big) \\
&\quad + \frac{h^\alpha}{\Gamma(\alpha+2)}\sum_{q=0}^{n} a_{q,n+1}\big(m_4 I(t_q) - \epsilon^\alpha D(t_q)\big) \\
P(t_{n+1}) &= P_0 + \frac{h^\alpha}{\Gamma(\alpha+2)}\big(\rho^\alpha I^p(t_{n+1}) + \theta^\alpha D^p(t_{n+1}) - m_5 P^p(t_{n+1})\big) \\
&\quad + \frac{h^\alpha}{\Gamma(\alpha+2)}\sum_{q=0}^{n} a_{q,n+1}\big(\rho^\alpha I(t_q) + \theta^\alpha D(t_q) - m_5 P(t_q)\big),
\end{aligned}\right\} \tag{24}$$

where:

$$\left.\begin{aligned}
S^p(t_{n+1}) &= S_0 + \frac{h^\alpha}{\Gamma(\alpha)}\sum_{q=0}^{n} b_{q,n+1}\big(\Lambda^\alpha - (\beta_1^\alpha I(t_q) + \beta_2^\alpha D(t_q) + \lambda^\alpha P(t_q))S(t_q) \\
&\quad +\phi^\alpha E(t_q) - m_1 S(t_q)\big), \\
E^p(t_{n+1}) &= E_0 + \frac{h^\alpha}{\Gamma(\alpha)}\sum_{q=0}^{n} b_{q,n+1}\big(\psi^\alpha S(t_q) - \gamma^\alpha(\beta_1^\alpha I(t_q) + \beta_2^\alpha D(t_q) \\
&\quad +\lambda^\alpha P(t_q))E(t_q) - m_2 E(t_q)\big), \\
I^p(t_{n+1}) &= I_0 + \frac{h^\alpha}{\Gamma(\alpha)}\sum_{q=0}^{n} b_{q,n+1}\big([(\beta_1^\alpha I(t_q) + \beta_2^\alpha D(t_q) + \lambda^\alpha P(t_q))S(t_q) \\
&\quad +\gamma^\alpha(\beta_1^\alpha I(t_q) + \beta_2^\alpha D(t_q) + \lambda^\alpha P(t_q))E(t_q)] - m_3 I(t_q)\big) \\
R^p(t_{n+1}) &= R_0 + \frac{h^\alpha}{\Gamma(\alpha)}\sum_{q=0}^{n} b_{q,n+1}\big(\sigma^\alpha I(t_q) - \mu^\alpha R(t_q)\big) \\
D^p(t_{n+1}) &= D_0 + \frac{h^\alpha}{\Gamma(\alpha)}\sum_{q=0}^{n} b_{q,n+1}\big(m_4 I(t_q) - \epsilon^\alpha D(t_q)\big) \\
P^p(t_{n+1}) &= P_0 + \frac{h^\alpha}{\Gamma(\alpha)}\sum_{q=0}^{n} b_{q,n+1}\big(\rho^\alpha I(t_q) + \theta^\alpha D(t_q) - m_5 P(t_q)\big).
\end{aligned}\right\} \tag{25}$$

In simulating the model (2) we assume the initial condition that $S(0) = 10000$, $E(0) = 290$, $I(0) = 10$, $R(0) = 50$, $D(0) = 0$ and $P(0) = 0$.

Table. 2. Parameters and values

Symbol	Definition	Range/ Value	Units	Source
δ	Disease death rate	0.4-0.9	day^{-1}	[50, 59, 60]
η	Environmental decontamination rate	0.06	day^{-1}	fitted
β_1	Transmission rate of infectious humans	variable	day^{-1}	[59, 61, 62]
β_2	Transmission rate of deceased humans	variable	day^{-1}	[60, 62]
λ	Transmission rate of Ebola virus	variable	day^{-1}	fitted
τ	Pathogen decay rate	$(0, \infty)$	day^{-1}	[63, 64]
ρ	Shading rate of infectious humans	0.0004	day^{-1}	fitted
θ	Shading rate of deceased humans	0.004	day^{-1}	fitted
ϵ	Burial rate of deceased humans	$(0, 1)$	day^{-1}	[62, 65]
μ	Natural death rate	$(0, 1)$	day^{-1}	[66]
ϕ	Lost of education rate	0.025	day^{-1}	fitted
γ	Modification factor	0.7	-	fitted
Λ	Recruitment rate	variable	day^{-1}	fitted
ψ	Education rate	0.31	day^{-1}	fitted
σ	Recovery rate of humans	$(0, 1)$	day^{-1}	[59, 61, 62]

4.2 Sensitivity Analysis

In this section, we perform the sensitivity analysis of the model (2). The threshold quantity $\mathcal{R}_0$ known as basic reproduction number is an important parameter to determine the persistence and extinction of EVD in the population. Parameter values of the Ebola model in Equation (2) taken from literature as presented in Table **??** and while some are estimated, therefore, sensitivity analysis will be useful on identifying parameters with greatest influence to change the magnitude of threshold quantity $\mathcal{R}_0$.

Definition 2. *(See, [67]) The normalized sensitivity index of $\mathcal{R}_0$ which depends on differentiability of parameter ω is defined as equation (26):*

$$\Psi_{\omega}^{\mathcal{R}_0} = \frac{\partial \mathcal{R}_0}{\partial \omega} \times \frac{\omega}{\mathcal{R}_0}, \tag{26}$$

where ω is the generic parameter of system (2).

Table. 3. Sensitivity index of the model (2)

Parameter	β_1	β_2	λ	ϕ
Index	+0.4154	+0.371	+0.2125	+0.0106
Parameter	σ	δ	ρ	θ
Index	-0.0107	-0.2939	+0.0023	+0.2102
Parameter	ψ	μ	γ	
Index	-0.0154	-0.1054	−0.1579	
Parameter	τ	η	ϵ	
Index	-0.008	0	-0.5823	

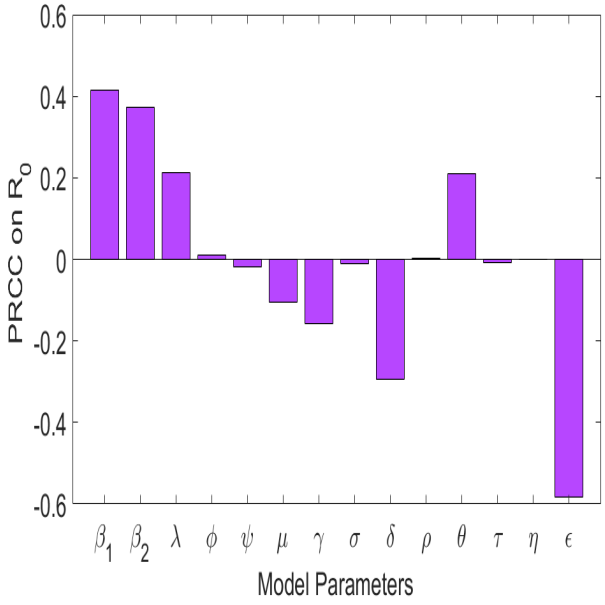

Fig. 2. Sensitivity index of the model (2)

We observed that model parameters such as β_1, β_2, λ, ϕ, ρ, and θ, have a positive influence on the magnitude of $\mathcal{R}_0$, that is, whenever they are increased, the magnitude of $\mathcal{R}_0$ increases. In Fig. 2. it can be observed that an increase in the values of β_1, β_2, λ, ϕ, ρ, and θ by 10% increases the magnitude of $\mathcal{R}_0$ by 4.154%, 3.721%, 2.125%, 0.106%, 0.023%, and 2.102%, respectively. While model parameters with negative index values have a negative influence on the magnitude of $\mathcal{R}_0$ an increase in the values of ψ, μ, γ, σ, δ, τ and ϵ by 10% decreases the magnitude of $\mathcal{R}_0$ by 0.154%, 1.054%, 1.579%, 0.107%, 2.939%, 0.08%, and 5.823%, respectively. These results suggest that the burial rate of deceased humans ϵ, has the highest negative influence on the magnitude of $\mathcal{R}_0$. In addition, an increase in the indirect transmission rate of Ebola virus λ, increases the magnitude of $\mathcal{R}_0$.

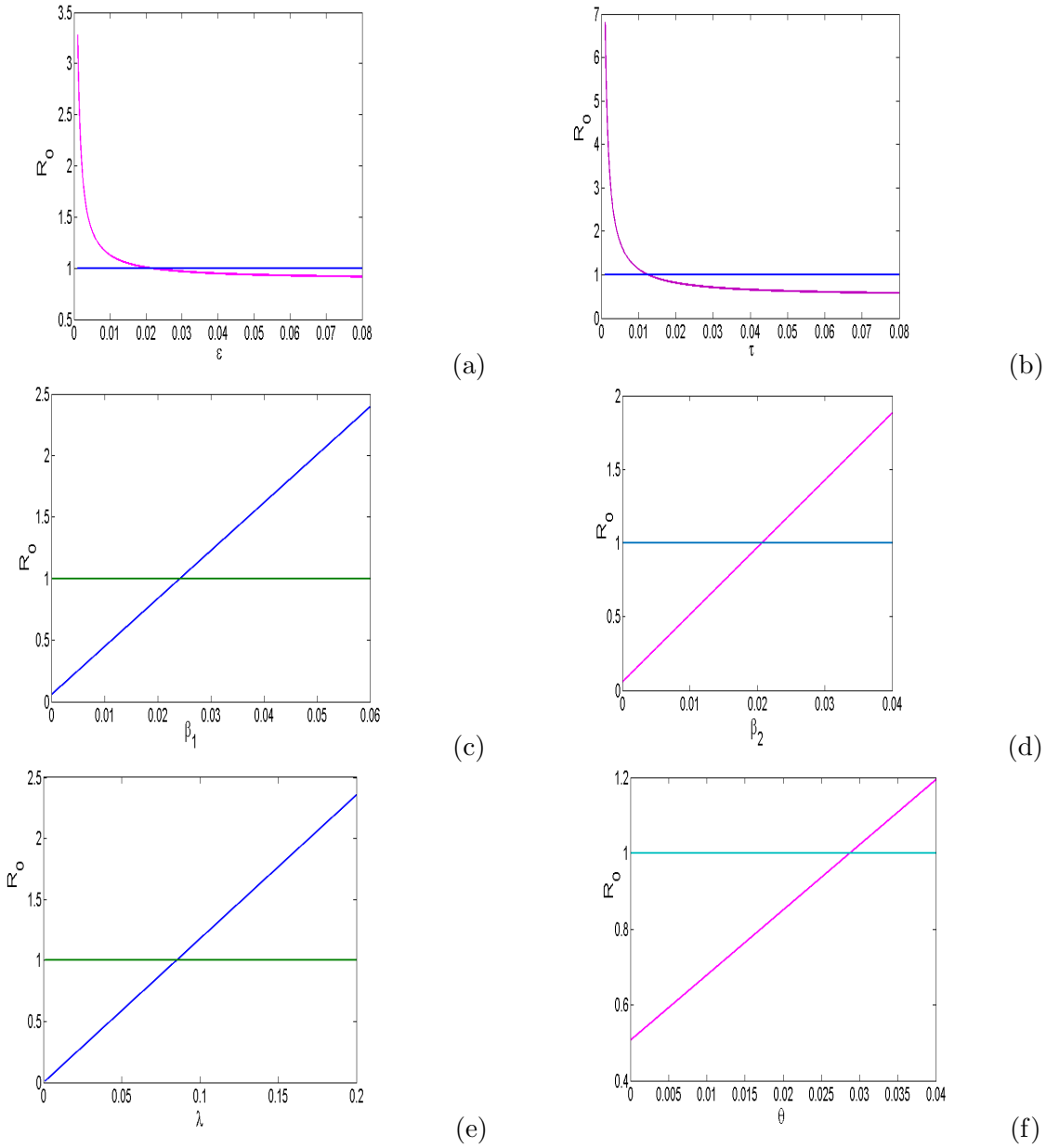

Fig. 3. Numerical results of model (2) showing effects of varying (a) burial rate of deceased humans ϵ, on $\mathcal{R}_0$ (b) pathogen decay rate of Ebola virus τ, on $\mathcal{R}_0$ (c) transmission rate from infectious human β_1, on $\mathcal{R}_0$ (d) transmission rate of deceased humans β_2, on $\mathcal{R}_0$ (e) transmission rate of Ebola virus λ, on $\mathcal{R}_0$ (f) shading rate of deceased humans θ, on $\mathcal{R}_0$.

We simulated model (2) to evaluate the effects of (a) burial rate of deceased humans ϵ, on $\mathcal{R}_0$, at different values of ϵ, (b) pathogen decay rate of Ebola virus τ, on $\mathcal{R}_0$, at different values of τ, (c) transmission rate from infectious human β_1, on $\mathcal{R}_0$, at different values of β_1 (d) transmission rate of deceased humans β_2, on $\mathcal{R}_0$, at

different values of β_2, (e) transmission rate of Ebola virus λ, on $\mathcal{R}_0$, at different values of λ (f) shading rate of deceased humans θ, on $\mathcal{R}_0$, at different values of θ. The other parameters are fixed in all cases as in Table 3.

The numerical results in Fig. 3 (a) show burial rate of deceased humans ϵ, on $\mathcal{R}_0$. We noted that increasing the burial rate on the deceased humans reduces the size of $\mathcal{R}_0$. Additionally, whenever ϵ is greater than 0.02, the EVD dies in the community. In Fig. 3 (b), we assess the effect of pathogen decay rate of Ebola virus τ, on $\mathcal{R}_0$. We noted that whenever $\tau > 0.01$, the disease dies in the population.

The numerical results in Fig. 3 (c) show transmission rate from infectious β_1, on $\mathcal{R}_0$. We noted that increasing the transmission rate from infectious human increases the magnitude of $\mathcal{R}_0$. In particular, whenever β_1 is greater than 0.025, the disease persists in the community. In Fig. 3 (d), we investigated the influence of transmission rate of deceased humans β_2, on $\mathcal{R}_0$. We observed that whenever $\beta_2 > 0.02$, the disease persists in the population.

The numerical results in Fig. 3 (e) show transmission rate of Ebola virus λ, on $\mathcal{R}_0$. We observed that increasing the transmission rate of Ebola virus increases the size of $\mathcal{R}_0$. In particular, whenever λ is greater than 0.1, the disease persists in the community. In Fig. 3 (f), we investigated the influence of shading rate of deceased humans θ, on $\mathcal{R}_0$. We noted that whenever $\theta > 0.03$, the disease persists in the community.

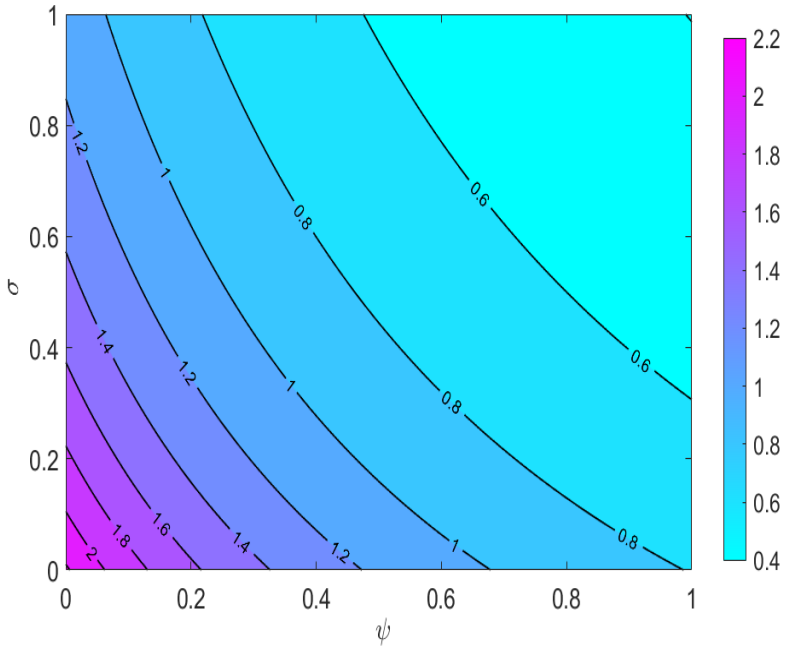

Fig. 4. Numerical results of model (2) showing contour graph of $\mathcal{R}_0$ as the function of prevention measures and educational campaigns. We simulated the model (2) at $\epsilon = 0.074, \quad \phi = 0.0004, \quad \beta_1 = 1 \times 10^{-8}$, and $\beta_2 = 9.7 \times 10^{-6}$.

Fig. 4. shows the contour graph of $\mathcal{R}_0$ as the function of educational campaigns and prevention measures. We simulated the model (2) at $\epsilon = 0.074, \quad \phi = 0.0004, \quad \beta_1 = 1 \times 10^{-8}$, and $\beta_2 = 9.7 \times 10^{-6}$. The results showed that as the rate of prevention measures and educational campaigns increases, the value of $\mathcal{R}_0$ decreases. This shows that both prevention measures and educational campaigns have the potential to reduce the spread of EVD in the community.

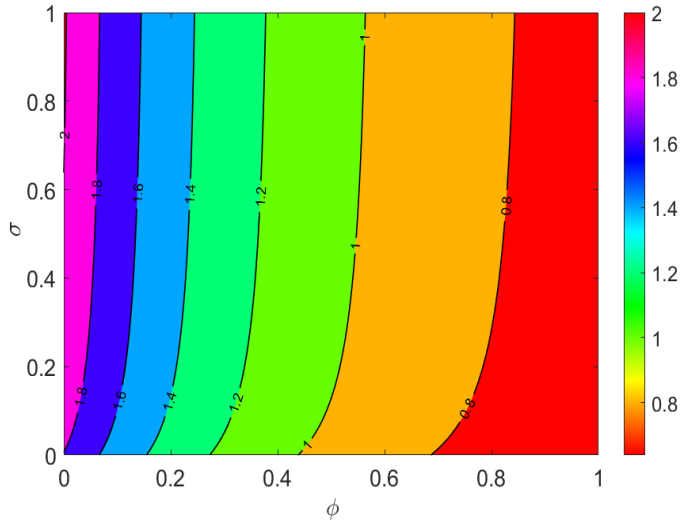

Fig. 5. Numerical results of model (2) showing contour graph of $\mathcal{R}_0$ as the function of prevention measures and treatment of infected individuals. We simulated the model (2) at $\epsilon = 0.08, \quad \psi = 0.025, \quad \beta_1 = 1 \times 10^{-8}$, and $\beta_2 = 9.7 \times 10^{-6}$.

Fig. 5. shows the contour graph of $\mathcal{R}_0$ as the function of prevention measures and recovery rate due to the treatment of infected individuals . We simulated the model (2) at $\epsilon = 0.08, \quad \psi = 0.025, \quad \beta_1 = 1 \times 10^{-8}$, and $\beta_2 = 9.7 \times 10^{-6}$. We observe that increasing the rate of prevention measures and recovery rate due to the treatment of infected individuals lead to decreased magnitude of $\mathcal{R}_0$. This demonstrates the effect of prevention measures and treatment of infected individuals in reducing the transmission of Ebola in the population.

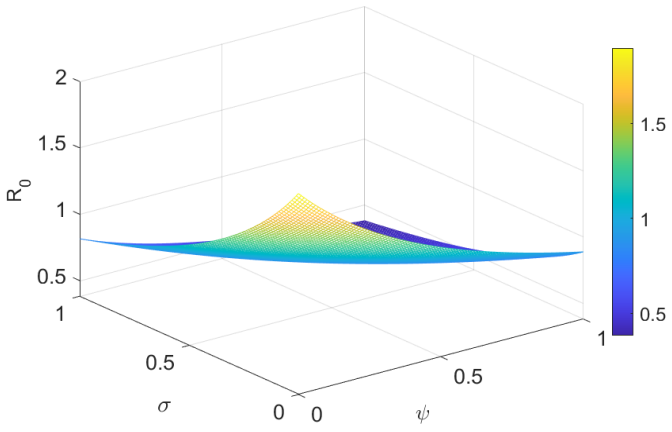

Fig. 6. Mesh plot of $\mathcal{R}_0$ as the function of educational campaigns and recovery rate due to the treatment of infected individuals. We simulated the model (2) at $\epsilon = 0.094, \quad \phi = 0.071, \quad \beta_1 = 1 \times 10^{-8}$, and $\beta_2 = 9.7 \times 10^{-6}$.

Fig. 6. shows the mesh plot of $\mathcal{R}_0$ as the function of educational campaigns and recovery rate due to the treatment of infected individuals . We simulated the model (2) at $\epsilon = 0.094, \quad \phi = 0.071, \quad \beta_1 = 1 \times 10^{-8}$, and $\beta_2 = 9.7 \times 10^{-6}$. It was noted that increasing the rate of educational campaigns and recovery rate due to the treatment of infected individuals lead to decreased magnitude of $\mathcal{R}_0$. This demonstrates the effect of educational campaigns and treatment of infected individuals reduce the transmission of Ebola in the population.

4.3 Parameter estimation

In this section, we numerically solve the proposed model (2) and estimate the parameters η, λ, ρ, θ, ϕ, γ, Λ, ψ that minimize the deviation of real data from the prediction model (2) using the least squares (RMSE) and Nelder mead algorithm techniques, and while the rest are fitted. The real data of Ebola cases used are reported in [9]. Despite the challenges in model fitting and parameter estimations, model fitting and parameter estimation in fractional order models is an integral part in the disease modeling. The present data were reported in Guinea from 22 March to 16 August 2014, and the cumulative new infections predicted by the model (2) is obtained using the equation (27):

$$D^{\alpha}_{t_0} C(t) \quad = \quad (\beta_1^{\alpha} I(t) + \beta_2^{\alpha} D(t) + \lambda^{\alpha} P(t))(S(t) + \gamma^{\alpha} E(t)) \tag{27}$$

Further, we use the following function to compute the best fitting:

$$\mathbb{F} : \mathbb{R}^{8}_{(\eta,\lambda,\rho,\theta,\phi,\gamma,\Lambda,\psi)} \to \mathbb{R}_{(\eta,\lambda,\rho,\theta,\phi,\gamma,\Lambda,\psi)} \tag{28}$$

where $\eta, \lambda, \rho, \theta, \phi, \gamma, \Lambda, \psi$ are variables such that:

(1) For a given $(\eta, \lambda, \rho, \theta, \phi, \gamma, \Lambda, \psi)$, solve numerically the model differential equations (2) to obtain a solution $\hat{Y}_i(t) = (\hat{S}, \hat{E}, \hat{I}, \hat{R}, \hat{P}, \hat{D})$ which is an approximation of the reported Ebola cases $Y(t)$.

(2) Set $t_0 = 1$ (the model fitting starts in March 22) and for $t = 2, 3, ..., 53$, corresponding to the number of weeks where data are available, obtain the computed numerical solution for $i_h(t)$; that is., $\hat{I}(1)$, $\hat{I}(2)$, $\hat{I}(3)$,....., $\hat{I}(53)$.

(3) Compute the (RMSE) of the difference between $\hat{I}(1), \hat{I}_h(2), ..., \hat{I}_h(53)$ and observed cases. This function $\mathbb{F}$ yields the RMSE where

$$\text{RMSE} = \sqrt{\frac{1}{n} \sum_{k=1}^{53} (I(k) - \hat{I}(k))^2}, \tag{29}$$

(4) By using Nelder-Mead algorithm determine a global minimum for the RMSE .

The function $\mathbb{F}$ takes values in $\mathbb{R}^8$ and yields a positive real number, the RMSE that measures the closeness of the model predictions to the observed data. Using the formula in equation (29), the $RMSE$ was found to be 0.1353. This shows that the proposed model had 13.53% deviations from observed values. It concluded that the model was approximately 86.47% efficient. On performing the fitting process, we assume the following initial conditions $S(0) = 1000$, $E(0) = 290$, $I(0) = 10$, $R(0) = 50$, $D(0) = 0$, and $P(0) = 0$ and the model parameters in Table 1.

Fig. 7. shows the cumulative detected cases of Ebola in Guinea. We used the monthly report of Ebola cases reported in [9] to fit the model (2) at $\alpha = 0.83$. The results demonstrated that the model (2) fits well the monthly Ebola cases reported in Guinea from 22 March to 16 August 2014.

The numerical results in Fig. 8(a) shows the real data fitted with the fractional model at the order of derivatives $\alpha = 0.81$, 0.82, 0.83, 0.84, 0.85. We noted that the model had better fit at $\alpha = 0.83$. Fig. 8(b), we plotted the variation of order of derivative against the sum of square error cumulative (SSEC). Overall, the model had minimum sum of square error cumulative at $\alpha = 0.83$ which agree with results in Fig. 8(b). Thus, the model had better fits at $\alpha = 0.83$.

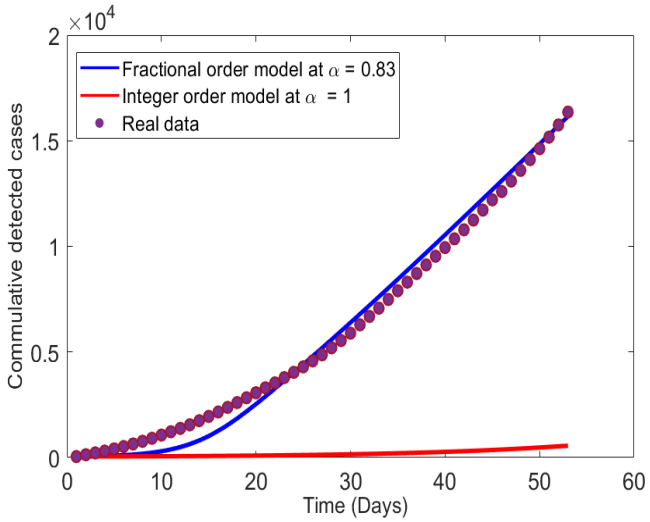

Fig. 7. The model (2) fitted to Ebola cases reported in Guinea from 22 March to 16 August 2014 at $\alpha = 0.83$.

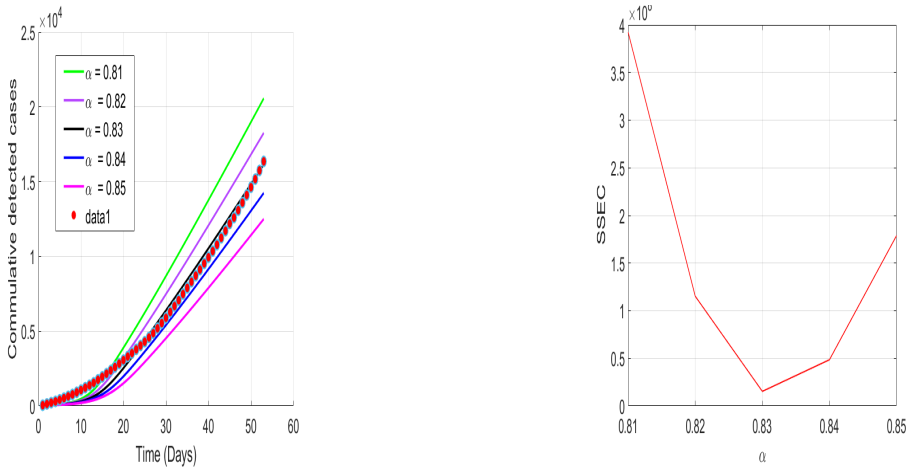

(a) (b)

Fig. 8. Numerical results of model 2 (a) shows the real data fitted at different order of derivatives (b) plots of order derivatives against the sum of square error cumulative (SSEC)

4.4 Numerical Results

Next, we simulate the model (2), we varied different model parameters and the order α of the caputo operator in order to explain the role of various parameters and memory index on the disease transmission patterns and control to support the analytical results. We first simulate the model at $\mathcal{R}_0 > 1$, followed by simulation at $\mathcal{R}_0 < 1$ to show the dynamics of the disease in the population.

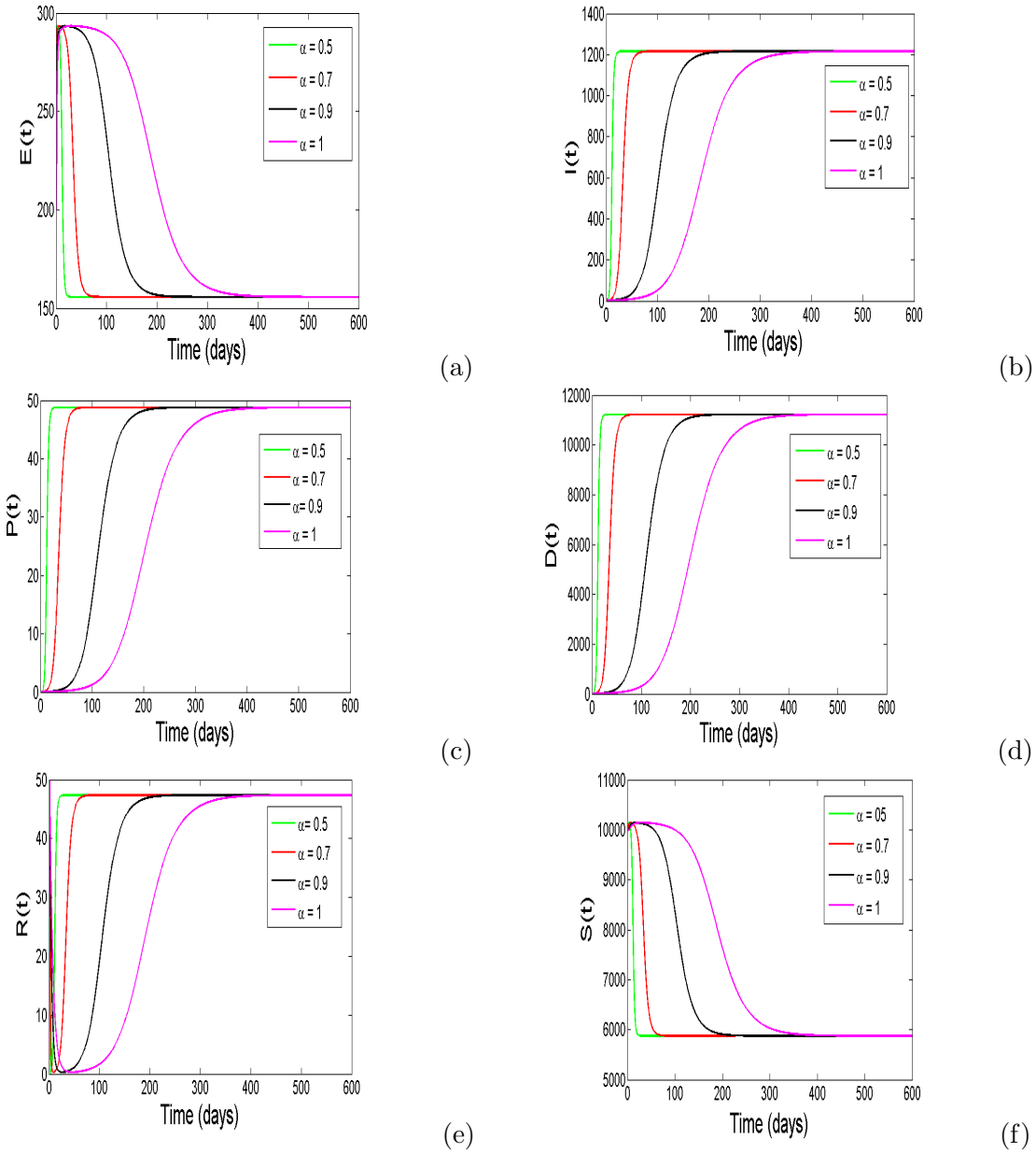

Fig. 9. Simulation of the model (2) showing the convergence of infected individuals at the endemic equilibria point.

Fig. 9. is a simulation of the model (2) to demonstrate the solution profile of individuals at the endemic equilibrium point. To explore the effects of different derivative orders, α, on the dynamics of the disease, we simulated the model at $\mathcal{R}_0 = 1.7520$, with the parameter values in Table 2 for $\alpha = 0.5$, $\alpha = 0.7$, $\alpha = 0.9$, and $\alpha = 1$. As we can note, with baseline values in Table 2, the disease will persist. Firstly, the results show that the variables for infected epidemiological compartments $I(t)$, $D(t)$, and $P(t)$ in Fig. 9 (b), 9 (c), and 9

(d) respectively, will increase the infection gradually and after about 300 days, the infection settle and attain stability at the endemic equilibrium at $I(t) \approx 1200$, $D(t) \approx 1050$, and $P(t) \approx 49$. A Similar pattern are observed for the compartment $R(t)$ in Fig. (9)(e). In addition, the variables for susceptible epidemiological compartments $S(t)$, and $E(t)$ in Fig. 9(a) and 9(f) respectively, show that susceptibility will decrease gradually and after about 300 days, the susceptibility settle and attain stability at the endemic equilibrium at $S(t) \approx 600$, and $E(t) \approx 290$. One can observe that as the value of the fractional-order α approaches unity, the time taken by model variables to converge to their respective unique endemic equilibrium point increases. These results agree with the analytical analysis of global stability for endemic equilibrium point in Theorem 3.4. It was further noted that at the fractional-order derivatives α, the human population attain its stability faster than at the classical integer.

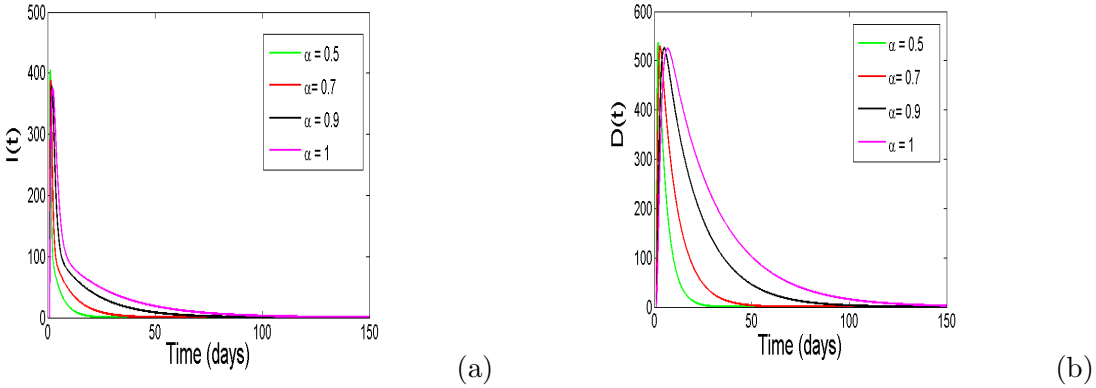

(a) (b)

Fig. 10. Simulation of the model (2) to show the convergence of infected humans and dead bodies at the disease free equilibrium point. We simulate the model (2) at $\mathcal{R}_0 = 0.6916$ with $\beta_1 = 1 \times 10^{-8}$, $\beta_2 = 9.7 \times 10^{-6}$, $\phi = 0.85$, $\psi = 0.71$. At different values of fractional-order derivatives, the number of infected individuals generated over the period of 150 days converge to the disease free equilibrium point.

Fig. 10. shows the simulation of the model (2) to demonstrate the convergence of infected human population to the disease-free equilibrium point. To examine the effects of different derivative orders, α, on the dynamics of the disease, we simulated the model at $\mathcal{R}_0 = 0.6916$, with $\beta_1 = 1 \times 10^{-8}$, $\beta_2 = 9.7 \times 10^{-6}$, $\phi = 0.85$, $\psi = 0.71$ and the remainder retained the baseline values in Table 2. for $\alpha = 0.5$, $\alpha = 0.7$, $\alpha = 0.9$, and $\alpha = 1$. As we can note, with baseline values in Table 2, the disease will die. We can note that, the variables for infected epidemiological compartments $I(t)$, and $D(t)$ in Fig. 10(a), and 10(b), respectively, show that the infection will decrease gradually and after about 100 days, the infection settle and attain stability at the disease-free equilibrium at $I(t) = 0$, and $D(t) = 0$. Furthermore, as the value of the fractional-order α approaches unity, the time taken by the model variables to converge to their respective unique disease-free equilibrium point increases. The results demonstrate that in a long-range interaction of people in the population, all infected individuals converge to one point which is the disease-free equilibrium point. This agrees with the analytical results on the existence of global stability for disease-free equilibrium point for the model (2) in Theorem 3.5. Also we have noted that as the fractional-order derivatives α decrease from integer and infected humans attain stability much faster than at $\alpha = 1$. This shows the importance of using fractional-order derivatives in modeling biological systems.

5 Concluding Remarks

In this article, a Caputo derivative model for EVD with intervention strategies is proposed and analyzed. A Majority of mathematical models for EVD in literature are based on integer-ordinary differential equations,

and much has not been done to investigate the role of memory effects on EVD dynamics. Thus, the main aim of this study was to develop a more realistic EVD model that incorporate memory effects. The formulated model subdivides the total human population based on epidemiological status as susceptible population unaware of the disease fighting, susceptible population aware of disease fighting; infected individuals who are clinically displaying signs of the disease and are infectious, individuals who have recovered from infection, and deceased population. The studied model has an additional compartment that captures the concentration of pathogens in the environment. We perform the sensitivity analysis to demonstrate the influence of each parameter on the magnitude of threshold quantity $\mathcal{R}_0$. The results show that that model parameters such as β_1, β_2, λ, ϕ, ρ, and θ, have a positive correlation with the magnitude of $\mathcal{R}_0$, that is, whenever they are increased, the magnitude of $\mathcal{R}_0$ increases. Furthermore, an increase in the values of β_1, β_2, λ, ϕ, ρ, and θ by 10% will increase the magnitude of $\mathcal{R}_0$ by 4.154%, 3.721%, 2.125%, 0.106%, 0.023%, and 2.102%, respectively. While model parameters with negative index values have a negative correlation with the magnitude of $\mathcal{R}_0$, we observed that an increase in the values of ψ, μ, γ, σ, δ, τ and ϵ by 10% decreases the magnitude of $\mathcal{R}_0$ by 0.154%, 1.054%, 1.579%, 0.107%, 2.939%, 0.08%, and 5.823%, respectively. These results suggest that the burial rate of deceased humans ϵ, has the highest negative influence on the magnitude of $\mathcal{R}_0$. In addition, an increase in the indirect transmission rate of Ebola virus λ, will increase the magnitude of $\mathcal{R}_0$.

The analytical results obtained in this study demonstrate that the fractional-order model has a globally asymptotically stable disease-free equilibrium whenever $\mathcal{R}_0 < 1$. However, if $\mathcal{R}_0 > 1$, the fractional-order model has an endemic equilibrium which is globally asymptotically stable.

Subsequently, we fitted the model parameters with the Ebola cases reported in Guinea from 22 March to 16 August 2014 at $\alpha = 0.82, 0.83, 0.84$ and 0.85. From our numerical results, the model fits well with cases reported and health education campaigns, prevention measures and treatments have the potential to minimize the spread of Ebola in the population. As the memory effect α decreases from unity, the solution profiles of the model (2) attain stability much faster than at $\alpha = 1$. In addition, the different values of the fractional-order have no effect on the stability of the model (2) but influence the time taken for stability to be attained. These results demonstrate the importance of fractional-order over the classical integer in modeling biological systems.

As the modelling of EVD is not sufficiently developed, this work offers many opportunities in improvements for future research where the model can be extended to incorporate a patch structure to account for the circulation of the disease in many countries as it is the case in Western Africa. In addition we expect to improve this study in the future by developing EVD model(s) with a time delay that will enable the comparison of the Caputo derivative and time delay approach.

Acknowledgment

All authors are grateful to their respective institutions for the support during preparation of the manuscript. Dr. Paride O. Lolika thank professor Yosa Wawa for his invaluable discussions and comments during the preparation of this manuscript.

Conflict of interest

The authors declare that they have no conflicts of interest

References

[1] Rouguet P, Bermejo JM, Kilbourne A, Karesh W, Reed P, Kumulunui B, Yaba P, Delicat A, Rollin PE, Leroy EM. Wild animal mortality monitoring and human Ebola outbreak, Gabon and Republic of Congo. 2001-2003. Emerg, Infect. Dis. 2005;11:283-290.

[2] Smith T. Ebola and Marbug Virus (Deadly Disease and epidemics), Second Ed. Chelsea House Pub; 2010.

[3] WHO. Ebola data and statistics; 2016.
Available: http://apps.who.int/gho/data/view.ebola-sitrep.ebola-summary-20160511?lang=en

[4] Jalloh MF, Li W, Bunnell RF, et al. Impact of Ebola experiences and risk perceptions on mental health in Sierra Leone, July 2015. BMJ Global Health. 2018;3:e000471.

[5] Richards P, Amara J, Ferme MC, Kamar P, Mokuwa E, Sheriff AI , Suluku R, Voors Marten M. Social pathways for Ebola virus disease in rural Sierra Leone and some implications for containment. PLOS Negl Trop Dis. 2014;8(7):e3056.

[6] Manguvo A, Mafuvadze B. The impact of traditional and religious practices on the spread of Ebola in West Africa: Time for a strategic shift. The Pan African Medical Journal. 22 Suppl 1(Suppl 1): 9.
DOI:10.11694/pamj.supp.2015;22.1.6190

[7] Hewlett Barry S, Amola Richard P. Cultural contexts of Ebola in northern Uganda. Emerg Infect Dis. 2003;9(10):1242.

[8] World Health Organization. Global alert and response; 2014.

[9] Althaus CL. Estimating the reproduction number of Ebola virus (EBOV) during the 2014 outbreak in West Africa. PLoS Currents Outbreaks. 2014;6.

[10] Barbarossa MV, Denes A, Kiss G, Nakata Y, R€ost G, Vizi Z. Transmission dynamics and final epidemic size of Ebola Virus Disease outbreaks with varying interventions. PLoS One. 2015;10(7):e0131398.

[11] Berge T, Lubuma JMS, Moremedi GM, Morris N, Kondera-Shava R. A simple mathematical model of Ebola in Africa. Journal of Biological Dynamics. 2017;11(1):42-74.
DOI: 10.1080/17513758.20161229817

[12] Bailey NTJ et al. The mathematical theory of infectious diseases and its applications. Charles Griffin & Company Ltd, 5a Crendon Street, High Wycombe, Bucks HP13 6LE; 1975.

[13] Anderson RM. The population dynamics of infectious diseases: Theory and applications. Springer; 2013.

[14] Thieme HR. Convergence results and a Poincare-Bendison trichotomy for asymptotical autonomous differential equations. J. Math. Biol. 1992;30:755-763.

[15] Wang W, Zhao XQ. Threshold dynamics for compartment epidemic models in periodic environments. Journal of Dynamics and Differential Equations. 2008;20:699-717.

[16] Dowel SF. Seasonal Variation in host susceptibility and cycles of certain infectious diseases. Emerging Infectious Diseases. 2001;7: 369-374.

[17] Shuai Z, Heesterbeek JAP, van den Driessche P. Extending the type reproduction number to infectious disease control targeting contacts between types. J. Math. Biol. 2013;67(5)1067-1082.

[18] Van den Driessche P, Watmough J. Reproduction number and subthreshold endemic equilibria for compartment models of disease transmission. Mathematical Biosciences. 2002;180:29-48.

[19] Erinle-Ibrahim Latifat M, Idowu KO, Sulola AI. Mathematical modelling of the transmission dynamics of malaria infection with optimal control. Kathmandu University Journal of Science, Engineering and Technology. 2021;15(3).

[20] Idowu KO, Loyinmi AC. Impact of contaminated surfaces on the transmission dynamics of corona virus disease (Covid-19). Journal of Science Techinical Research; 2023.
DOI: 10.26717/BJSTR.2023.51.008046

[21] Idowu KO, Erinle-Ibrahim LM. Mathematical modelling of pneumonia dynamics of children under the age of five. Research Square; 2021.
DOI: https://doi.org/10.21203/rs.3.rs-194578/v1

[22] Idowu KO, Loyinmi AC. Qualitative analysis of the transmission dynamics. Research Square, and Optimal Control of Covid-19; 2023.
DOI: https://doi.org/10.21203/rs.3.rs-2707554/v1

[23] Saeedian M, Khalighi M, Azimi-Tafreshi N, Jafari GR, Ausloos M. Memory effects on epidemic evolution: The susceptible-infected-recovered epidemic model. Physical Review E. 2017;95(2):022409.

[24] Hamdan N, Kilicman A. Analysis of the fractional order dengue transmission model: A case study in Malaysia. Springer. 2019;1:1-13.

[25] Mouaouine A, Boukhouima A, Hattaf K, Yousfi N. A fractional order SIR epidemic model with nonlinear incidence rate. Springer. 2018;1-9.

[26] Liu JG, Yang XJ, Feng YY, Geng LL. Fundamental results to the weighted Caputo-type differential operator. Applied Mathematics Letters. 2021;121:107421.

[27] Rihan FA, Al-Mdallal QM, AlSakaji HJ, Hashish A. A fractional-order epidemic model with time-delay and nonlinear incidence rate. Elsevier. 2019;126:97-105.

[28] Vargas-De-Leó n. Volterra-type Lyapunov functions for fractional-order epidemic systems. Commun, Nonlinear Sci. Numer. Simul. 2015;24:75-85.

[29] Helikumi M, Kgosimore M, Kuznetsov D, Mushayabasa S. A fractional-order Trypanosoma brucei rhodesiense model with vector saturation and temperature dependent parameters. Springer. 2020;1:1-23.

[30] Area I, Batarfi H, Losada J, Nieto JJ, Shammakh W, Torres A. On a fractional order Ebola epidemic model. Advances in Difference Equations. 2015(1):1-12.

[31] Farman M, Akgül A, Abdeljawad T, Naik PA, Bukhari N, Ahmad A. Modeling and analysis of fractional order Ebola virus model with Mittag-Leffler kernel. Elsevier. 2022;61(3):2061-2073.

[32] Dokuyucu MA, Dutta H. A fractional order model for Ebola Virus with the new Caputo fractional derivative without singular kernel. Elsevier. 2020;134:109717.

[33] Raza A, Farman M, Akgül A, Iqbal MS, Ahmad A. Simulation and numerical solution of fractional order Ebola virus model with novel technique. AIMS Bioengineering. 2020;7(4):194-207.

[34] Singh H. Analysis for fractional dynamics of Ebola virus model. Chaos, Solitons & Fractals. 2020;138:109992.

[35] Pan W, Li T, Ali S. A fractional order epidemic model for the simulation of outbreaks of Ebola. Springer. 2021;1-21.

[36] Li HL, Zhang L, Hu C, Jiang YL, Teng Z. Dynamical analysis of a fractional-order predator-prey model incorporating a prey refuge. Journal of Applied Mathematics and Computing. 2017;54(1-2):435-449.

[37] de Barros LC, Lopes MM, Santo Pedro F, Esmi E, dos Santos JPC, Sánchez DE. The memory effect on fractional calculus: An application in the spread of COVID-19. Computational and Applied Mathematics. 2021;40(3):1-21.

[38] Huo J, Zhao H, Zhu L. The effect of vaccines on backward bifurcation in a fractional order HIV model. Nonlinear Analysis: Real World Applications. 2015;26:289-305.

[39] Naik PA, Zu J, Owolabi KM. Global dynamics of a fractional order model for the transmission of HIV epidemic with optimal control. Chaos, Solitons & Fractals. 2020;138:109826.

[40] Owolabi KM. Behavioural study of symbiosis dynamics via the Caputo and Atangana–Baleanu fractional derivatives. Chaos, Solitons & Fractals. 2019;122:89-101.

[41] Owolabi KM, Atangana A. Mathematical analysis and computational experiments for an epidemic system with nonlocal and nonsingular derivative. Chaos, Solitons & Fractals. 2019;126:41-49.

[42] Zafar ZUA, Rehan K, Mushtaq M. HIV/AIDS epidemic fractional-order model. Journal of Difference Equations and Applications. 2017;23(7):1298-1315.

[43] Muhammad Altaf K, Atangana A. Dynamics of Ebola disease in the framework of different fractional derivatives. Entropy. 2019;21(3):303.

[44] Juan Z, Zhien M. Global dynamics of an seir epidemic model with saturating contact rate. Mathematical Biosciences Journal. 2003;185:15-32.

[45] Nielsen Carie F, Kidd S, Sillah AR, Davis E, Mermin J, Kilmarx Peter H. Improving burial practices and cemetery management during an Ebola virus disease epidemic-Sierra Leone, 2014. MMWR. 2015;64(1):20.

[46] Berhe HW, Qureshi S, Shaikh AA. Deterministic modeling of dysentery diarrhea epidemic under fractional Caputo differential operator via real statistical analysis. Chaos, Solitons & Fractals. 2020;131:109536.

[47] Alkahtani BS. Atangana-Batogna numerical scheme applied on a linear and non-linear fractional differential equation. The European Physical Journal Plus. 2018;133(3):1-10.

[48] Huo J, Zhao H, Zhu L. The effect of vaccines on backward bifurcation in a fractional order HIV model. Nonlinear Analysis: Real World Applications. 2015;26:289-305.

[49] Delavari H, Baleanu D, Sadati J. Stability analysis of Caputo fractional-order. Nonlinear Systems Revisited, Nonlinear Dyn. 2012;67:2433-2439.

[50] Aguston FB, Teboh-Wwaungkem MI, Gumel AB. Mathematical assessment of the effect of traditional beliefs and customs on the transmission dynamics of the 2014 Ebola outbreak. BMC MED. 2015;13:96.

[51] Ivorra B, Ngom D, Ramos AM, Be-CodiS. A mathematical model to predict the risk of human diseases spread between countries-validation and application to the 2014-2015 ebola virus disease epidemic. Bull. Math. Bio. 2015;77:1668-1704.

[52] Li C, Zeng F. The finite difference methods for fractional ordinary differential equations. Numer Funct Anal Optim. 2013;34:149-179.
DOI: https://doi.org/10.1080/01630563.2012.706673

[53] Liang S, Wu R, Chen L. Laplace transform of fractional order differential equations. Electron J Differ Equ. 2015;139.
Available: http://ejde.math.txstate.edu

[54] Kexue L, Jigen P. Laplace transform and fractional differential equations. Appl Math Lett. 2011;24:2019-2023.
DOI: https://doi.org/10.1016/j.aml.2011.05.035

[55] Podlubny I. Fractional differential equations: An introduction to fractional derivatives, fractional differential equations, to methods of their solution and some of their applications. Math Sci Eng. 1999;7:1-340.
DOI: https://doi.org/10.1016/s0076-5392(99)x8001-5

[56] Chen M, Wu R. Dynamics of a depletion-type Gierer-Meinhardt model with Langmuir- Hinshelwood reaction scheme. Discrete and Continuous Dynamical Systems Series B. 2022; 27(4):2275-2312.

[57] Khalil HK. Nonlinear Systems (Third edition), Prentice Hall, Englewood Cliffs, NJ; 2002.

[58] Diethelm K. The analysis of fractional differential equations: An application-oriented exposition using differential operators of caputo type. Springer Science & Business Media; 2020.

[59] Chowell G, Hengartner NW, Castillo-Chavez C, Fenimore PW, Hyman JM. The basic reproductive number of Ebola and the effects of public health measures: The cases of Congo and Uganda. J. Theo. Biol. 2014;229:119-126.

[60] Fisman D, Khoo E, Tuite A. Early epidemic dynamics of the the West African 2014 Ebola outbreak: Estimates derived with a simple two Parameter model. PLOS Curr. outbreaks. Edition 1; 2014.
DOI: 10.1371/89cod3783f36958d96ebbae97348d571

[61] Legrand J, Grais RF, Boelle PY, Valleron AJ, Flahault A. Understanding thd dynamics of Ebola epidemics. Epidemiol. Infect. 2007;135:610-621.

[62] Towers S, Patterson-Lomba O, Castillo-Chavez C. Temporal variations in the reproduction number of the 2014 outbreaks. PLOS Curr. Outbreaks. September 18; 2014.

[63] Bibby K, Casson LW, Stachler E, Haas CN. Ebola virus persistence in the environment state of the knowledge and research needs. Envoron. Sci. Technol. Lett. 2. 2015;2-6.

[64] Piercy TJ, Smither SJ, Steward JA, Eastaugh L, Lever MS. The survival of filoviruses in liquids, on solid substrate and in a dynamic aerosol. J. App. Microbio. 2010;109(5):1531-1539.

[65] Fasina FO, Shitu A, Lazarus D, Tomori O, Simonsen L, Viboud C, Chowell G. Transmission dynamics and control of Ebola virus disease outbreak in Nigeria, July to September 2014. Euro Surviell. 2014;19(40):20920. Available : http://www.eurosurveillance.org/ ViewAricle.spxa?Articled=20920

[66] Ndanguza D, Tchuenche JM, Haario H. Statistical data analysis of the 1995 outbreak in the Democratic Republic of Congo. Afrika Mat. 2013;24:55-68.

[67] Arriola L, Hyman J. Forward and adjoint sensitivity analysis with applications in dynamical systems. Lecture Notes in Linear Algebra and Optimization; 2005.

Appendix

Appendix A: Mathematical concepts of fractional order

Consider the following differential equation of any dynamical system:

$$\frac{df(t)}{dt} = \beta f(t) \tag{30}$$

where β is any constant or parameter. In order to capture the influence of memory effects, we rewrite the differential equation (30) in terms of dependent integral as follows:

$$\frac{df(t)}{dt} = \beta \int_{t_0}^{t} k(t-\xi) f(\xi) d\xi \tag{31}$$

In this case, $k(t-\xi)$ plays the role of the time dependent kernel and is equivalent to a delta $\delta(t-\xi)$ in a classical Markov process. This type of kernel provides the existence of important features which exist in real problems. Now let us consider the following power-law correlation function for $k(t-\xi)$:

$$k(t-\xi) = \frac{1}{\Gamma(\alpha-1)}(t-\xi)^{\alpha-2} \tag{32}$$

where $\Gamma(\alpha)$ denotes the Gamma function and $0 < \alpha \leq 1$. In this case, the choice of coefficient $\Gamma(\alpha-2)$ and the exponent $\alpha-1$ allow to write the differential equation (30) to the form of fractional order derivative in Caputo sense. Substituting this kernel in (30) the right hand side of function leads to the fractional integral of order $(\alpha-1)$ on the interval $[b,t]$, denoted by ${}_bD_{t_0}^{-(\alpha-1)}$. Applying a fractional Caputo derivative of order $(\alpha-1)$ in (30) and using the fact that both Caputo fractional derivative and fractional integral are inverse operators, one gets the following fractional differential equation:

$$D_{t_0}^{\alpha} f(t) = \beta^{\alpha} f(t) dt \tag{33}$$

where $D_{t_0}^{\alpha} f(t)$ denotes the Caputo fractional derivative of order $\alpha \in (0,1)$, defined for an arbitrary function $f(t)$ as:

$$D_{t_0}^{\alpha} f(t) = \frac{1}{\Gamma(1-\alpha)} \int_0^t \frac{\dot{f}(\xi)}{(t-\xi)^{\alpha}} d\xi. \tag{34}$$

Thus, the function (34) defines the fractional order derivatives in Caputo sense.
Remarks : Note that, In order to avoid flaws regarding the time dimension, we introduce the α in parameter β (right-hand side) of the differential equation (33) so that the dimension of the parameter β become $(time)^{-\alpha}$ which agree with the left-hand side of the differential equation.

Definition 3. *For the differential equation described in (30)*

(i) The trivial solution is said to be stable if, for every $t_0 \in \mathbb{R}$ and every $\epsilon > 0$, there exists $\delta = \delta(t_0, \epsilon)$ such that $||x(t_0)|| < \delta \rightarrow ||x(t)|| < \epsilon$ for all $t > t_0$.

(ii) The trivial solution is said to be symptomatically stable if it is stable and, for any $t_0 \in \mathbb{R}$ and any $\epsilon > 0$, there exists $\delta_a = \delta_a(t_0, \epsilon) > 0$ such that $||x(t)|| < \delta_a \rightarrow \lim_{t\to\infty} ||x(t)|| = 0$

(iii) The trivial solution is said to be uniformly stable if it is stable and $\delta = \delta(\epsilon) > 0$ can be chosen independently of t_0.

(iv) The trivial solution is uniformly symptomatically stable if it is uniformly stable and there exists δ_a independently of t_0, such that if $||x(t)|| < \delta_a$, then $\lim_{t\to\infty} ||x(t)|| = 0$.

(iii) The trivial solution is said to be uniformly stable if it is stable and $\delta = \delta(\epsilon) > 0$ can be chosen independently of t_0.

(v) The trivial solution is globally symptomatically stable if it is symptomatically stable and δ_a can be any arbitrarily large finite number.

Appendix B: Non-negativity and boundedness of model solutions

In this section, we present the existence, uniqueness, positivity and boundedness of the solutions of model (2). We commence our discussion by demonstrating existence and uniqueness of solutions. Our approach is based on the fixed-point theory. Let $\mathcal{B}$ be a Banach space of real-valued continuous functions defined on an interval $\mathcal{I}$ with the associated norm:

$$\|S, E, I, R, D, P\| = \|S\| + \|E\| + \|I\| + \|R\| + \|D\| + \|P\| \tag{35}$$

where $\|S\| = \sup\{|S(t)| : t \in \mathcal{I}$, $\|E\| = \sup\{|E(t)| : t \in \mathcal{I}$, $\|I\| = \sup\{|I(t)| : t \in \mathcal{I}$, $\|R\| = \sup\{|R(t)| : t \in \mathcal{I}$, $\|D\| = \sup\{|D(t)| : t \in \mathcal{I}$, $\|P\| = \sup\{|P(t)| : t \in \mathcal{I}$, and $\mathcal{B} = \mathcal{E}(\mathcal{I}) \times \mathcal{E}(\mathcal{I}) \times \mathcal{E}(\mathcal{I}) \times \mathcal{E}(\mathcal{I}) \times \mathcal{E}(\mathcal{I}) \times \mathcal{E}(\mathcal{I}) \times \mathcal{E}(\mathcal{I})$, with $\mathcal{E}(\mathcal{I})$ denoting the Banach space of real-valued continuous functions on $\mathcal{I}$ and the associated sup norm. The model system (2) can be rewritten in the the following form:

$$\left.\begin{array}{rcl} D^{\alpha}_{t_0} S(t) &=& G_1(t, S), \\ D^{\alpha}_{t_0} E(t) &=& G_2(t, E), \\ D^{\alpha}_{t_0} I(t) &=& G_3(t, I), \\ D^{\alpha}_{t_0} R(t) &=& G_4(t, R), \\ D^{\alpha}_{t_0} D(t) &=& G_5(t, D), \\ D^{\alpha}_{t_0} P(t) &=& G_6(t, P), \end{array}\right\}. \tag{36}$$

By applying the Caputo fractional integral operator, system (36), reduces to the following integral equation of Volterra type with Caputo fractional integral of order $0 < \alpha < 1$,

$$\left.\begin{array}{rcl} S(t) - S(0) &=& \frac{1}{\Gamma(\alpha)} \int_0^t (t-\chi)^{\alpha-1} G_1(\chi, S) d\chi, \\ E(t) - E(0) &=& \frac{1}{\Gamma(\alpha)} \int_0^t (t-\chi)^{\alpha-1} G_2(\chi, E) d\chi, \\ I(t) - I(0) &=& \frac{1}{\Gamma(\alpha)} \int_0^t (t-\chi)^{\alpha-1} G_3(\chi, I) d\chi, \\ R(t) - R(0) &=& \frac{1}{\Gamma(\alpha)} \int_0^t (t-\chi)^{\alpha-1} G_4(\chi, I) d\chi, \\ D(t) - D(0) &=& \frac{1}{\Gamma(\alpha)} \int_0^t (t-\chi)^{\alpha-1} G_5(\chi, D) d\chi, \\ P(t) - P(0) &=& \frac{1}{\Gamma(\alpha)} \int_0^t (t-\chi)^{\alpha-1} G_6(\chi, P) d\chi, \end{array}\right\} \tag{37}$$

What follows, we prove that the kernels G_i, $i = 1, 2, 3, 4, 5, 6$ fulfill the Lipschitz condition and contraction under some assumptions. In the following theorem, we have demonstrated for G_1 and one can easily verify for the remainder.

Theorem 5.1. *Let us consider the following inequality*

$$0 \leq (\beta_1 k_1 + \beta_2 k_2 + \lambda k_3 + \mu + \psi) < 1.$$

The kernel G_1 satisfies the Lipschitz condition as well as contraction if the above inequality is satisfied.

Proof. For S and S_1 we proceed as below.

$$\begin{array}{rcl} \|G_1(t, S) - G_1(t, S_1)\| &=& \| - ((\beta_1 k_1 + \beta_2 k_2 + \lambda k_3 + \mu + \psi)))(S(t) - S_1(t)) \\ &=& (\mu + \psi)\|S - S_1\| + \beta_1 I + \beta_2 D + \lambda P)\|(S - S_1)\|. \end{array} \tag{38}$$

Since $I(t)$, $D(t)$ and $P(t)$ are bounded functions, i.e, $\|I\| \leq k_1\|$, $\|D\| \leq k_2$ and $\|P\| \leq k_3$, by the property of norm functions, the above inequality (38) can be written as

$$\|G_1(t, S) - G_1(t, S_1)\| \leq \eta_1 \|S(t) - S_1(t)\|, \tag{39}$$

where $\eta_1 = \beta_1 k_1 + \beta_2 k_2 + \lambda k_3 + \mu + \psi$. Hence for G_1 the Lipschitz condition is obtained and if an additionally $0 \leq \beta_1 k_1 + \beta_2 k_2 + \lambda k_3 + \mu + \psi < 1$, we obtain a contraction. The Lipschitz condition for the other kernels are

$$\left.\begin{array}{rcl} \|G_2(t, E) - G_2(t, E_1)\| &\leq& \eta_2 \|E(t) - E_1(t)\|, \\ \|G_3(t, I) - G_3(t, I_1)\| &\leq& \eta_3 \|I(t) - I_1(t)\|, \\ \|G_4(t, R) - G_4(t, R_1)\| &\leq& \eta_4 \|R(t) - R_1(t)\|, \\ \|G_5(t, D) - G_5(t, D_1)\| &\leq& \eta_5 \|D(t) - D_1(t)\|, \\ \|G_6(t, P) - G_6(t, P_1)\| &\leq& \eta_6 \|P(t) - P_1(t)\|, \end{array}\right\} \tag{40}$$

□

Recursively, the expression in (37) can be written as

$$\left.\begin{array}{lcl} S_n(t)-S(0) &=& \frac{1}{\Gamma(\alpha)}\int_0^t (t-\chi)^{\alpha-1}G_1(\chi,S_{n-1})d\chi, \\ E_n(t)-E(0) &=& \frac{1}{\Gamma(\alpha)}\int_0^t (t-\chi)^{\alpha-1}G_2(\chi,E_{n-1})d\chi, \\ I_n(t)-I(0) &=& \frac{1}{\Gamma(\alpha)}\int_0^t (t-\chi)^{\alpha-1}G_3(\chi,I_{n-1})d\chi, \\ R_n(t)-R(0) &=& \frac{1}{\Gamma(\alpha)}\int_0^t (t-\chi)^{\alpha-1}G_4(\chi,R_{n-1})d\chi, \\ D_n(t)-D(0) &=& \frac{1}{\Gamma(\alpha)}\int_0^t (t-\chi)^{\alpha-1}G_5(\chi,D_{n-1})d\chi, \\ P_n(t)-P(0) &=& \frac{1}{\Gamma(\alpha)}\int_0^t (t-\chi)^{\alpha-1}G_6(\chi,P_{n-1})d\chi, \end{array}\right\} \tag{41}$$

The difference between successive terms of system (36) in recursive form is given below:

$$\left.\begin{array}{lcl} \phi_{1n} &=& S_n(t)-S_{n-1}(t) \\ &=& \frac{1}{\Gamma(\alpha)}\int_0^t (t-\chi)^{\alpha-1}(G_1(\chi,S_{n-1})-G_1(\chi,S_{n-2}))d\chi, \\ \phi_{2n} &=& E_n(t)-E_{n-1}(t) \\ &=& \frac{1}{\Gamma(\alpha)}\int_0^t (t-\chi)^{\alpha-1}(G_2(\chi,E_{n-1})-G_2(\chi,E_{n-2}))d\chi, \\ \phi_{3n} &=& I_n(t)-I_{n-1}(t) \\ &=& \frac{1}{\Gamma(\alpha)}\int_0^t (t-\chi)^{\alpha-1}(G_3(\chi,I_{n-1})-G_3(\chi,I_{n-2}))d\chi, \\ \phi_{4n} &=& R_n(t)-R_{n-1}(t) \\ &=& \frac{1}{\Gamma(\alpha)}\int_0^t (t-\chi)^{\alpha-1}(G_4(\chi,R_{n-1})-G_4(\chi,R_{n-2}))d\chi, \\ \phi_{5n} &=& D_n(t)-D_{n-1}(t) \\ &=& \frac{1}{\Gamma(\alpha)}\int_0^t (t-\chi)^{\alpha-1}(G_5(\chi,D_{n-1})-G_5(\chi,D_{n-2}))d\chi, \\ \phi_{6n} &=& P_n(t)-P_{n-1}(t) \\ &=& \frac{1}{\Gamma(\alpha)}\int_0^t (t-\chi)^{\alpha-1}(G_6(\chi,P_{n-1})-G_6(\chi,P_{n-2}))d\chi, \end{array}\right\} \tag{42}$$

with the initial conditions $S_0(t)=S(0)$, $E_0(t)=E(0)$, $I_0(t)=I$, $R_0(t)=R(0)$, $D_0(t)=D(0)$ and $P_0(t)=P_0$. Taking the norm of the first equation of (42), we obtain

$$\begin{aligned} \|\phi_{1n}(t)\| &= \|S_n(t)-S_{n-1}(t)\| \\ &= \|\frac{1}{\Gamma(\alpha)}\int_0^t (t-\chi)^{\alpha-1}(G_1(\chi,S_{n-1})-G_1(\chi,S_{n-2}))d\chi\| \\ &\leq \frac{1}{\Gamma(\alpha)}\|\int_0^t (t-\chi)^{\alpha-1}(G_1(\chi,S_{n-1})-G_1(\chi,S_{n-2}))d\chi\|. \end{aligned} \tag{43}$$

Applying the Lipschitz condition (39) one gets

$$\|S_n(t)-S_{n-1}(t)\| \leq \frac{1}{\Gamma(\alpha)}\eta_1\int_0^t (t-\chi)^{\alpha-1}\|S_{n-1}-S_{n-2}\|d\chi. \tag{44}$$

Thus, we have

$$\|\phi_{1n}(t)\| \leq \frac{1}{\Gamma(\alpha)}\eta_1\int_0^t (t-\chi)^{\alpha-1}\|\phi_{1n}(t)\|d\chi. \tag{45}$$

Similarly, for the remainder of the equations in system (2) we have

$$\left.\begin{array}{lcl} \|\phi_{2n}(t)\| &\leq& \frac{1}{\Gamma(\alpha)}\eta_2\int_0^t (t-\chi)^{\alpha-1}\|\phi_{2n}(t)\|d\chi, \\ \|\phi_{3n}(t)\| &\leq& \frac{1}{\Gamma(\alpha)}\eta_3\int_0^t (t-\chi)^{\alpha-1}\|\phi_{3n}(t)\|d\chi, \\ \|\phi_{4n}(t)\| &\leq& \frac{1}{\Gamma(\alpha)}\eta_4\int_0^t (t-\chi)^{\alpha-1}\|\phi_{4n}(t)\|d\chi, \\ \|\phi_{5n}(t)\| &\leq& \frac{1}{\Gamma(\alpha)}\eta_5\int_0^t (t-\chi)^{\alpha-1}\|\phi_{5n}(t)\|d\chi, \\ \|\phi_{6n}(t)\| &\leq& \frac{1}{\Gamma(\alpha)}\eta_6\int_0^t (t-\chi)^{\alpha-1}\|\phi_{6n}(t)\|d\chi, \end{array}\right\} \tag{46}$$

From (46) one can write

$$\left.\begin{array}{llll} S_n(t) = \sum_{i=1}^{n} \phi_{1i}(t), & E_n(t) = \sum_{i=1}^{n} \phi_{2i}(t), & I_n(t) = \sum_{i=1}^{n} \phi_{3i}(t), \\ R_n(t) = \sum_{i=1}^{n} \phi_{4i}(t), & D_n(t) = \sum_{i=1}^{n} \phi_{5i}(t), & P_n(t) = \sum_{i=1}^{n} \phi_{6i}(t), \end{array}\right\} \tag{47}$$

Now, we claim the following result which guaranteed the uniqueness of solution of model (2).

Theorem 5.2. *The proposed fractional epidemic model (2) has a unique solution for $t \in [0, T]$ if the following inequality holds*

$$\frac{1}{\Gamma(\alpha)} b^{\alpha} \eta_i < 1, \qquad i = 1, 2, ..., 7. \tag{48}$$

Proof. Earlier we have shown that the kernels conditions given in Eqs. (39) and (40) holds. Thus by considering the Eqs. (46) and (48), and by applying the recursive technique we obtained the succeeding results as below:

$$\left.\begin{array}{rcl} \|\phi_{1n}(t)\| & \leq & \|S_0(t)\| \left[\frac{1}{\Gamma(\alpha)} b^{\alpha} \eta_1\right]^n, \quad \|\phi_{2n}(t)\| \leq \|E_0(t)\| \left[\frac{1}{\Gamma(\alpha)} b^{\alpha} \eta_2\right]^n, \\ & & \|\phi_{3n}(t)\| \leq \|I_0(t)\| \left[\frac{1}{\Gamma(\alpha)} b^{\alpha} \eta_3\right]^n, \\ \|\phi_{4n}(t)\| & \leq & \|R_0(t)\| \left[\frac{1}{\Gamma(\alpha)} b^{\alpha} \eta_4\right]^n, \quad \|\phi_{5n}(t)\| \leq \|D_0(t)\| \left[\frac{1}{\Gamma(\alpha)} b^{\alpha} \eta_5\right]^n, \\ & & \|\phi_{6n}(t)\| \leq \|P_0(t)\| \left[\frac{1}{\Gamma(\alpha)} b^{\alpha} \eta_6\right]^n, \end{array}\right\} \tag{49}$$

Therefore, the above mentioned sequences exist and satisfy $\|\phi_{1n}(t)\| \to 0$, $\|\phi_{2n}(t)\| \to 0$, $\|\phi_{3n}(t)\| \to 0$, $\|\phi_{4n}(t)\| \to 0$, $\|\phi_{5n}(t)\| \to 0$, and $\|\phi_{6n}(t)\| \to 0$. Furthermore, from Eq. (49) and employing the triangle inequality for any k, we one gets

$$\left.\begin{array}{l} \|S_{n+k}(t) - S_n(t)\| \leq \sum_{j=n+1}^{n+k} T_1^j = \frac{T_1^{n+1} - T_1^{n+k+1}}{1 - T_1}, \\ \|E_{n+k}(t) - E_n(t)\| \leq \sum_{j=n+1}^{n+k} T_2^j = \frac{T_2^{n+1} - T_2^{n+k+1}}{1 - T_2}, \\ \|I_{n+k}(t) - I_n(t)\| \leq \sum_{j=n+1}^{n+k} T_3^j = \frac{T_3^{n+1} - T_3^{n+k+1}}{1 - T_3}, \\ \|R_{n+k}(t) - R_n(t)\| \leq \sum_{j=n+1}^{n+k} T_4^j = \frac{T_4^{n+1} - T_4^{n+k+1}}{1 - T_4}, \\ \|D_{n+k}(t) - D_n(t)\| \leq \sum_{j=n+1}^{n+k} T_5^j = \frac{T_5^{n+1} - T_5^{n+k+1}}{1 - T_5}, \\ \|P_{n+k}(t) - P_n(t)\| \leq \sum_{j=n+1}^{n+k} T_6^j = \frac{T_6^{n+1} - T_6^{n+k+1}}{1 - T_6}, \end{array}\right\} \tag{50}$$

where $T_i = \frac{1}{\Gamma(q)} b^q \eta_i < 1$ by hypothesis. Therefore, S_n, E_n, I_n, R_n, D_n and P_n are regardedas Cauchy sequences in the Banach space $B(J)$. Hence they are uniformly convergent as described in [52]. Applying the limit theory on Eq. (41) when $n \to \infty$ affirms that the limit of these sequences is the unique solution of system (2). Ultimately, the existence of a unique solution for system (2) has been achieved. □

We now demonstrate the positivity of solutions for all $t \geq 0$. To prove positivity and boundedness of solutions, we need the following Generalized Mean Value Theorem in [**?**] and corollary.

Lemma 1. *Suppose that $f(x) \in C[a,b]$ and $D^{\alpha}_{t_0} f(x) \in C[a,b]$, for $0 < \alpha \leq 1$, then we have*

$$f(x) = f(a) + \frac{1}{\Gamma(\alpha)} (D^{\alpha}_{t_0} f)(\xi)(x-a)^{\alpha} \tag{51}$$

with $a \leq \xi x$, $\forall x \in (a,b]$ and $\Gamma(\cdot)$ is the gamma function.

Corollary 1. *Suppose that $f(x) \in C[a,b]$ and $D^{\alpha}_{t_0} f(x) \in C(a,b]$, for $0 < \alpha \leq 1$. If $D^{\alpha}_{t_0} f(x) \geq 0$, $\forall x \in (a,b)$, then $f(x)$ is non-decreasing for each $x \in [a,b]$. If $D^{\alpha}_{t_0} f(x) \leq 0$, $\forall x \in (a,b)$, then $f(x)$ is non-increasing for each $x \in [a,b]$.*

We now prove that the non-negative orthant $\mathbb{R}^6_+$ is positively invariant region. To do this, we need to show that on each hyperplane bounding the non-negative orthant, the vector field points to $\mathbb{R}^6_+$. From model (2), one gets:

$$\begin{aligned}
D^{\alpha}_{t_0} S(t)|_{S=0} &= \Lambda^{\alpha} \geq 0, && (52)\\
D^{\alpha}_{t_0} E(t)|_{E=0} &= \psi^{\alpha} S(t) \geq 0, && (53)\\
D^{\alpha}_{t_0} I(t)|_{I=0} &= (\beta_1^{\alpha} I(t) + \beta_2^{\alpha} D(t) + \lambda^{\alpha} P(t))(S(t) + \gamma^{\alpha} E(t)) \geq 0, && (54)\\
D^{\alpha}_{t_0} R(t)|_{R=0} &= \sigma^{\alpha} I(t) \geq 0, && (55)\\
D^{\alpha}_{t_0} D(t)|_{D=0} &= (\mu^{\alpha} + \delta^{\alpha}) I(t) \geq 0, && (56)\\
D^{\alpha}_{t_0} P(t)|_{P=0} &= \rho^{\alpha} I(t) + \theta^{\alpha} D(t) \geq 0, && (57)
\end{aligned}$$

Thus, by Corollary 1, the solution of model (2) are always positive for $t \geq 0$. We now demonstrate that all solutions of model (2) are bounded above for all $t \geq 0$. To do this, we need the following Lemma 2 and Lemma 3.

Lemma 2. *(see [53]). Let $\alpha > 0$, $n-1 < \alpha < n - \mathbb{N}$. Suppose that $f(t), f'(t), ..., f^{(n-1)}(t)$ are continuous on $[t_0, \infty)$ and the exponential order and that $D^{\alpha}_{t_0} f(t)$ is piecewise continuous on $[t_0, \infty)$. Then*

$$\mathcal{L}\{D^{\alpha}_{t_0} f(t)\} = s^{\alpha} \mathcal{F}(s) - \sum_{k=0}^{n-1} s^{\alpha-k-1} f^{(k)}(t_0) \tag{58}$$

where $\mathcal{F}(s) = \mathcal{L}\{f(t)\}$.

Lemma 3. *(see [54]). Let $\mathbb{C}$ be the complex plane. For any $\alpha > 0$ $\beta > 0$, and $A \in \mathbb{C}^{n \times n}$, we have*

$$\mathcal{L}\{t^{\beta-1} E_{\alpha,\beta}(At^{\alpha})\} = s^{\alpha-\beta}(s^{\alpha} - A)^{-1},$$

for $\mathcal{R}s > \|A\|^{\frac{1}{\alpha}}$, where $\mathcal{R}s$ represents the real part of the complex number s, and $E_{\alpha,\beta}$ is the Mittag-Leffler function [55].

Since all solutions of model system (2) have been shown to be positively invariant and have a lower bound zero (52)-(57), we now proceed to demonstrate that these solutions are bounded above. By summing all equations of system (2) one gets:

$$\begin{aligned}
D^{\alpha}_{t_0} N(t) &= \Lambda^{\alpha} - \mu^{\alpha} N(t) - \epsilon^{\alpha} D(t) - (\tau^{\alpha} + \eta^{\alpha}) P(t)\\
&\leq \Lambda^{\alpha} - \mu^{\alpha} N(t). && (59)
\end{aligned}$$

Taking the Laplace transform of (59) leads to:

$$s^{\alpha} \mathcal{L}(N(t)) - s^{\alpha-1} N(0) \leq \frac{\Lambda^{\alpha}}{s} - \mu^{\alpha} \mathcal{L}(N(t)). \tag{60}$$

Combining like terms and arranging leads to

$$\mathcal{L}(N(t)) \leq \Lambda^{\alpha} \frac{s^{-1}}{s^{\alpha} + \mu^{\alpha}} + N(0) \frac{s^{\alpha-1}}{s^{\alpha} + \mu^{\alpha}}$$

$$= \Lambda^{\alpha}\frac{s^{\alpha-(1+\alpha)}}{s^{\alpha}+\mu^{\alpha}} + N(0)\frac{s^{\alpha-1}}{s^{\alpha}+\mu^{\alpha}}. \tag{61}$$

Applying the inverse Laplace transform leads to

$$\begin{aligned} N(t) &\leq \mathcal{L}^{-1}\left\{\Lambda^{\alpha}\frac{s^{-1}}{s^{\alpha}+\mu^{\alpha}} + N(0)\frac{s^{\alpha-1}}{s^{\alpha}+\mu^{\alpha}}\right\} + \mathcal{L}^{-1}\left\{N(0)\frac{s^{\alpha-1}}{s^{\alpha}+\mu^{\alpha}}\right\} \\ &\leq \Lambda^{\alpha}t^{\alpha}E_{\alpha,\alpha+1}(-\mu t^{\alpha}) + N(0)E_{\alpha,1}(-\mu t^{\alpha}) \\ &\leq \frac{\Lambda^{v}}{\mu^{\alpha}}\mu^{\alpha}t^{\alpha}E_{\alpha,\alpha+1}(-\mu t^{\alpha}) + N(0)E_{\alpha,1}(-\mu t^{\alpha}) \\ &\leq \max\left\{\frac{\Lambda^{\alpha}}{\mu^{\alpha}}, N(0)\right\}(\mu^{\alpha}t^{\alpha}E_{\alpha,\alpha+1}(-\mu t^{\alpha}) + E_{\alpha,1}(-\mu t^{\alpha})) \\ &= \frac{C}{\Gamma(1)} = C, \end{aligned} \tag{62}$$

where $C = \max\left\{\frac{\Lambda^{\alpha}}{\mu^{\alpha}}, N(0)\right\}$. Thus, $N(t)$ is bounded from above. This completes the proof of Theorem (3.1).

Peer-review history:
The peer review history for this paper can be accessed here (Please copy paste the total link in your browser address bar)
http://www.sdiarticle5.com/review-history/110718